

**PRELIMINARY RESULTS FROM A TWO-MOMENT
AEROSOL MODEL APPLIED TO A
THREE-DIMENSIONAL MODEL OF THE
GLOBAL SULFUR CYCLE**

Sonia M. Kreidenweis and Debra Y. Harrington

**Department of Atmospheric Science
Colorado State University
Fort Collins, CO**

John J. Walton and Joyce E. Penner

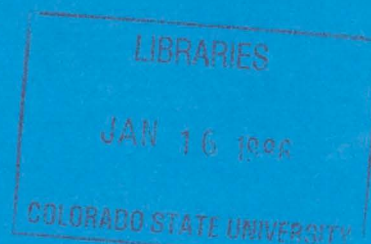
**Lawrence Livermore National Laboratory
Livermore, CA**

Funding Agency:

National Science Foundation #ATM-9215951

December, 1995

**Colorado
State
University**



**DEPARTMENT OF
ATMOSPHERIC SCIENCE**

PAPER NO. 594

**Preliminary Results from a
Two-Moment Aerosol Model Applied to a
Three-Dimensional Model of the
Global Sulfur Cycle**

Sonia M. Kreidenweis

Debra Y. Harrington

Department of Atmospheric Science
Colorado State University
Fort Collins, CO

John J. Walton

Joyce E. Penner

Lawrence Livermore National Laboratory
Livermore, CA



018401 4069511

QC
852
C6
no. 594
ATMOS

Abstract

The focus of this work is the development and application of a two-mode, two-moment model of sulfate aerosol dynamics that is coupled to the Lawrence Livermore National Laboratory (LLNL) three dimensional transport, transformation, and deposition model, GRANTOUR. The new aerosol model predicts two moments of the distribution, particle number concentration and particle mass concentration; earlier studies of the global sulfur cycle have predicted only a single moment of the aerosol, the total mass of particulate sulfate. Two modes are used to represent the fine aerosol fraction in this study. The treatment of sulfuric acid vapor is also modified from earlier studies, from a diagnostic variable usually set equal to zero, to a prognostic variable which drives the gas-to-particle conversion in the aerosol model. The parameterized two-moment aerosol model was developed for computational efficiency and the small number of prognostic variables, which reduce storage requirements in the large-scale model. The addition of this simple aerosol scheme nearly tripled the computational time needed to complete a month of simulation, relative to that for a chemistry-only run.

The implementation of the aerosol model in GRANTOUR is described, and preliminary steady-state results from perpetual July simulations are presented and discussed. Anthropogenic and natural sources of sulfur gases were used as input, with simple oxidation schemes converting the gases to sulfuric acid. No direct emissions of particulate matter or other sources of aerosol mass were considered. Predictions of aerosol sulfate mass concentrations at the surface are nearly identical to previous results from the single-moment aerosol scheme, and are highest in industrialized regions with large anthropogenic emissions. However, the spatial distribution of number concentration is markedly different from that for the particulate mass. In particular, the predicted monthly mean surface number concentrations in continental regions are much lower than observations. This result is interpreted as indicating that direct emissions of particulate matter are the strongest regulator of particle number concentration in such regions, and must be included to improve comparisons with observations. At 355 mb, however, the predicted number concentrations are generally higher than those at the surface, and show a latitudinally-banded structure similar to some observations. This result is interpreted as signifying a lessening of the importance of surface primary emissions in determining the number concentrations of free tropospheric aerosol.

A trajectory analysis is performed for one parcel which was lifted to a 300 mb height after picking up emissions in the marine boundary layer of the western North Atlantic. Several thousand particles cm^{-3} were nucleated in this parcel in the free troposphere. It was later brought to the surface in subsiding air over northern Africa, where it contributed to an unexpectedly high monthly mean number concentration in this region. The analysis, although limited in scope, supports the idea that the free troposphere may serve as a source of aerosol number to the boundary layer.

1. Introduction

There has been increased recognition of the importance of aerosols in climate change and climate prediction. Aerosols affect the climate both directly, through scattering and absorption of incoming solar radiation, and indirectly, through their ability to act as cloud condensation nuclei (CCN). Recent studies (Charlson *et al.*, 1991; Kiehl and Briegleb, 1993) suggest that the effects of aerosols may be similar in magnitude, but opposite in sign, to the projected global warming attributed to greenhouse gas accumulation.

Such calculations indicate the need for an improved understanding of the mechanisms regulating atmospheric aerosol formation and evolution before accurate assessments of the climate impacts of changes in aerosol precursor gases can be made. The importance of aerosols to climate suggests that the indirect and direct effects of aerosols must be included in general circulation models. In order to estimate the effect of perturbations in aerosol sources and sinks upon global atmospheric aerosol concentrations, major sources of particles and their precursor gases must be incorporated into large-scale models, and a method must be developed for describing the conversion of gases to particulate matter.

One approach to examining aerosol climate effects is to consider individually the different chemical constituents which comprise the atmospheric aerosol. Sulfate compounds have been of particular interest for a number of reasons: they generally constitute a major mass fraction of particulate matter; sulfur has both natural and anthropogenic sources; sulfates are efficient scatterers of radiation; and soluble sulfate compounds are expected to enhance the cloud-nucleating ability of particles containing them. The modeling of the global cycle of sulfur, including the distribution of particulate sulfur species, is important in developing an understanding of the relative importance of natural and anthropogenic sulfur sources, and in computing the radiative effects of these compounds.

Some aspects of the radiative effects, including the calculation of optical properties and the availability of particles which can serve as cloud condensation nuclei, require knowledge of the number concentration and size of aerosol particles. Previous models of the global sulfur cycle have used sulfur source inventories, simple chemical conversion rate equations, and parameterized wet and dry removal rate for gases and particulate matter to predict global aerosol sulfate mass loadings (*e.g.*, Langner and Rodhe, 1991). For the purposes of computing properties needed to estimate radiative effects, particle size

distributions must be assumed, and the number concentration is then diagnosed from the mass concentration (*e.g.*, Erickson *et al.*, 1991).

In their three-dimensional global sulfur model, Langner and Rodhe (1991) predicted particulate sulfate mass concentrations which were used by Charlson *et al.* (1991) and Kiehl and Briegleb (1993) in their estimates of aerosol direct radiative effects. Charlson *et al.* (1991) applied representative mass scattering efficiencies to the predicted sulfate mass concentrations; Kiehl and Briegleb (1993) and Chuang and Penner (1994) assumed particle size distributions and determined corresponding aerosol number concentrations for computing optical and CCN properties. Both approaches are useful for obtaining estimates of present-day aerosol radiative effects, and these studies demonstrated that the climate effects of aerosols are substantial enough to warrant additional study (Penner *et al.*, 1994b). Assessment of the potential for change in such estimates, however, is more difficult. Aerosol size distributions should respond to local sources and sinks of particles, and indeed significant temporal and spatial variability in aerosol distributions is observed (d'Almeida *et al.*, 1991). Thus, in further developing understanding of how the atmospheric aerosol will respond to changes in source strength, sink strength, the temporal and spatial distribution of both, and other processes that influence the aerosol, a method is needed for predicting not only particulate mass production and loss rates, but also particulate number production and loss. In this report, we present results from a model formulation which represents a first step in developing such capability.

The focus of this work is the development of a simple two-moment, two-mode model of sulfate aerosol dynamics that has been coupled to a three dimensional global sulfur chemistry transport, transformation, and deposition model. The two-moment model was chosen based on computational efficiency and the small number of prognostic variables, which reduce storage requirements in the large-scale model. The five prognostic variables used are the sulfuric acid vapor concentration and the mass and number concentration of two modes of the aerosol distribution, both considered to be in the fine (submicron) aerosol fraction. In developing the two-moment aerosol scheme, comparison with a sectional model approach was used to derive several of the parameterized rates. Details of these parameterizations are discussed in Youngblood and Kreidenweis (1994) and are described only briefly here.

The implementation of the aerosol model in the LLNL GRANTOUR model is described, and results are discussed with respect to processes which determine aerosol number in the global aerosol model. The atmospheric aerosol cannot be fully described by a sulfate-only treatment, particularly near the surface over continents where significant additional sources of aerosol number and submicron mass exist. However, even this simplified treatment yields interesting observations with respect to aerosol transport and aerosol mass and number relationships. Sensitivity studies for some of the parameterized rates used are also shown. The comparisons of some of these preliminary model results with observations are used to suggest additional features that should be added to the aerosol model to bring the predictions more in line with observations.

2. Model description

2.1 GRANTOUR transport

GRANTOUR is a global transport, transformation and deposition model which has been applied to 3-D tropospheric chemistry studies (Walton *et al.*, 1988; Erickson *et al.*, 1991; Penner *et al.*, 1994a; Galloway *et al.*, 1992). It is formulated as a Lagrangian parcel model, typically run with 50,000 air parcels which represent constant air mass parcels in the atmosphere. Each parcel carries trace constituents represented by mass mixing ratios.

Advection of the parcels is carried out on an Eulerian grid with 4.5° latitude and 7.5° longitude grid spacing, and twelve vertical levels defined by pressure coordinates (sigma levels). The model can be run off-line by using wind and precipitation data from a GCM, or can be run interactively, allowing species to alter the wind and precipitation fields. The off-line method was used in this study, with 12 hour averaged meteorology obtained from CCM1 model runs.

A time-splitting technique is used to separate the transport from the chemical and microphysical calculations; these are computed on the Lagrangian parcels, which carry the chemical and aerosol species information. Advection is first carried out for a model timestep. After the advection timestep is completed, the new positions of parcels with respect to the Eulerian grid are analyzed and are used to obtain new emissions source rates and wet and dry deposition rates. A diffusional mixing scheme is also applied, as described below. Chemical and microphysical calculations are then performed for the same

total timestep; the choice of integration timestep within the chemistry / microphysics module is discussed further in later sections.

Although nearly all of the transport rate expressions are identical to those used in previous GRANTOUR modeling studies, the existing diffusional mixing scheme was modified as follows to accommodate the two-moment aerosol model. In the non-particulate versions of the model the change in mass mixing ratio of a species is computed at the model's Eulerian nodes and is mapped onto the parcels. In this new version, mass mixing ratio (kg kg^{-1}) is treated as before, while the change in number mixing ratio (kg^{-1}) is not computed independently, but rather is related to changes in mass. This is necessary since, if particle mass is removed from a parcel, the number of particles consistent with this mass must be removed. If the moments are instead diffused or advected independently, inconsistent ratios of N and M can result. In the two-moment treatment, all parcels independently compute total mass and number of particulate matter, so that the mean size is not fixed; thus, the particulate mass which is assumed to be added to a parcel as a result of diffusional mixing is added as a mixture of particles of varying sizes. To estimate the typical particle mass entering, the current background values are interpolated to the parcel from the Eulerian grid. If M and N are the background mass and number mixing ratios of one of the aerosol modes at the parcel, and ΔM is the change in mass mixing ratio at the parcel, then ΔN , the applied change in particle number at the parcel, is

$$\Delta N = \Delta M \frac{N}{M}. \quad (1)$$

2.2 GRANTOUR chemistry

The species that have been included in the global sulfur cycle model are sulfur dioxide (SO_2), hydrogen sulfide (H_2S) (represented as DMS), dimethylsulfide (DMS), and sulfuric acid (H_2SO_4), also called "sulfate" here. The gaseous emissions are treated in three families, grouped by source type. The first sulfur branch is made up of SO_2 and its oxidation product, H_2SO_4 , and is driven by anthropogenic SO_2 sources. The second is made up of DMS and its oxidation products SO_2 and H_2SO_4 , and is driven by natural sources which include oceanic, vegetation, and soil sources of DMS and vegetation and

soil sources of H₂S. The third branch, driven by volcanic sources of SO₂, is made up of SO₂ and its oxidation product H₂SO₄. All sources are imposed at the center of grid boxes and, except for the volcanoes, are assumed to be well mixed in the lowest 100 mb. The volcanoes are assumed to be well mixed throughout the appropriate vertical domain. Table 1 lists the various sources, their July injection rates, and their vertical domain in terms of sigma whose value increases towards the surface.

Table 1. Trace gas sources and emissions rates included in modeling study.

Source	July Injection (kg month ⁻¹)	Domain (sigma level)
SO ₂ volcano 0 – 3 km	2.0457×10^8	0.7 – 1.0
SO ₂ volcano 0 – 6 km	3.0704×10^8	0.5 – 1.0
SO ₂ volcano 0 – 9 km	4.2605×10^7	0.3 – 1.0
SO ₂ biomass burning	5.4762×10^8	0.9 – 1.0
SO ₂ anthropogenic	1.2453×10^{10}	0.9 – 1.0
DMS ocean	3.4437×10^9	0.9 – 1.0
DMS soil	4.4656×10^6	0.9 – 1.0
DMS vegetation	2.7822×10^7	0.9 – 1.0
H ₂ S soil	6.2006×10^6	0.9 – 1.0
H ₂ S vegetation	1.8340×10^8	0.9 – 1.0

The gaseous emissions are oxidized by reaction with OH· or via a highly simplified aqueous-phase pathway (Table 2). The reaction rate coefficients shown in Table 2 are varied according to the average temperature and pressure at each location in the model. The aqueous reaction is assumed to proceed, with a characteristic e-folding time of 30 hours modified by a factor which scales as the square of the ratio of local [OH·] to the surface [OH·] at 40° N in summer (Penner *et al.*, 1994a). The aerosol model treats the aqueous-

phase pathway as mass input directly to the aerosol phase, with no net increase in number. The background OH· field is specified according to diurnally-averaged and latitudinally - and seasonally-varying concentrations calculated from the LLNL-2D model (Wuebbles *et al.* 1987). The origin of the emissions rates used, their spatial distributions, the determination of the OH· distribution, and the wet and dry deposition rates used are described fully in Penner *et al.* (1994a).

Table 2. *Oxidation reactions and rates constants used in the model. All species are gas-phase unless otherwise noted.*

Reaction	Rate constant (at 298 K)
DMS + OH· → SO ₂	k = 6.13 x 10 ⁻¹² cm ³ s ⁻¹
SO ₂ + OH· → H ₂ SO ₄ (g)	k = 8.89 x 10 ⁻¹³ cm ³ s ⁻¹
H ₂ S + OH· → SO ₂	k = 6.13 x 10 ⁻¹² cm ³ s ⁻¹
SO ₂ → H ₂ SO ₄ (aerosol)	k = 9.26 x 10 ⁻⁶ s ⁻¹

As seen from Table 2, the sulfur chemistry used is sufficiently simple that it is possible to write analytic solutions to the source-chemistry equations. In previous model implementations, 6-hour timesteps were used to integrate the chemical source terms. The inclusion of the aerosol model necessitates more frequent updating of the source rate of sulfuric acid vapor, so that a 1-hour coupling timestep between chemistry and aerosol processes is utilized.

2.3 Two-moment aerosol model

2.3.a Conceptual overview

The chemical mechanism described in Section 2.2 is essentially the same as that used in prior implementations of the GRANTOUR sulfur cycle model. However, in earlier work,

all H_2SO_4 was assumed to exist in the particulate phase. The present version redefines this variable as the gas-phase sulfuric acid species, and adds new variables to describe the particulate sulfate; the partitioning between vapor and aerosol phases is computed in the new aerosol module. This may be thought of as a modification from the previous diagnostic scheme for the H_2SO_4 (g) concentration (which set this quantity to zero) to a prognostic scheme for that species (Figure 1). In addition, the two-moment aerosol model now also partitions the mass and number concentrations of particulate H_2SO_4 into two aerosol size modes. Thus, the inclusion of the aerosol model adds four new variables to the existing seven chemical species: N_1 , M_1 , N_2 , and M_2 , the aerosol number and mass mixing ratios in modes 1 and 2, respectively. It should be noted that the prognosed mass mixing ratios are for H_2SO_4 (*aer*) only, although additional species, notably liquid water in the aerosol phase, are accounted for in some of the rate expressions, as discussed below.

The bimodal structure simulates accumulation and nucleation mode particles in the fine particle fraction of the aerosol; a representation of coarse mode particulate matter is not yet included. Indeed, since this study is restricted to sulfate aerosols, the mass and number concentrations of particulate sulfate are the only aerosol species explicitly carried. Clearly this approach will underestimate both the number and mass of the atmospheric aerosol, as interpreted in the sensitivity study later. This treatment represents the first steps in developing the capability for prognostic vapor calculations, allowing for differences in particle formation and growth rates in different regions of the atmosphere, and in developing a framework for the prediction of aerosol number concentration.

It is important to note that the same source and sink rates, including wet and dry deposition rates for H_2SO_4 , are used in the model runs with and without the explicit aerosol module. Thus, as seen in Figure 1, for the steady-state results which will be shown and discussed, the same magnitudes and spatial distribution of total sulfate (vapor + particulate) mass mixing ratios are expected in both cases. However, particulate number mixing ratios are also prognosed in those runs performed with the aerosol model, and the distribution of aerosol number concentration will be to a certain extent independent of the distribution of aerosol mass concentration; thus the mass mean particle size will vary spatially and temporally.

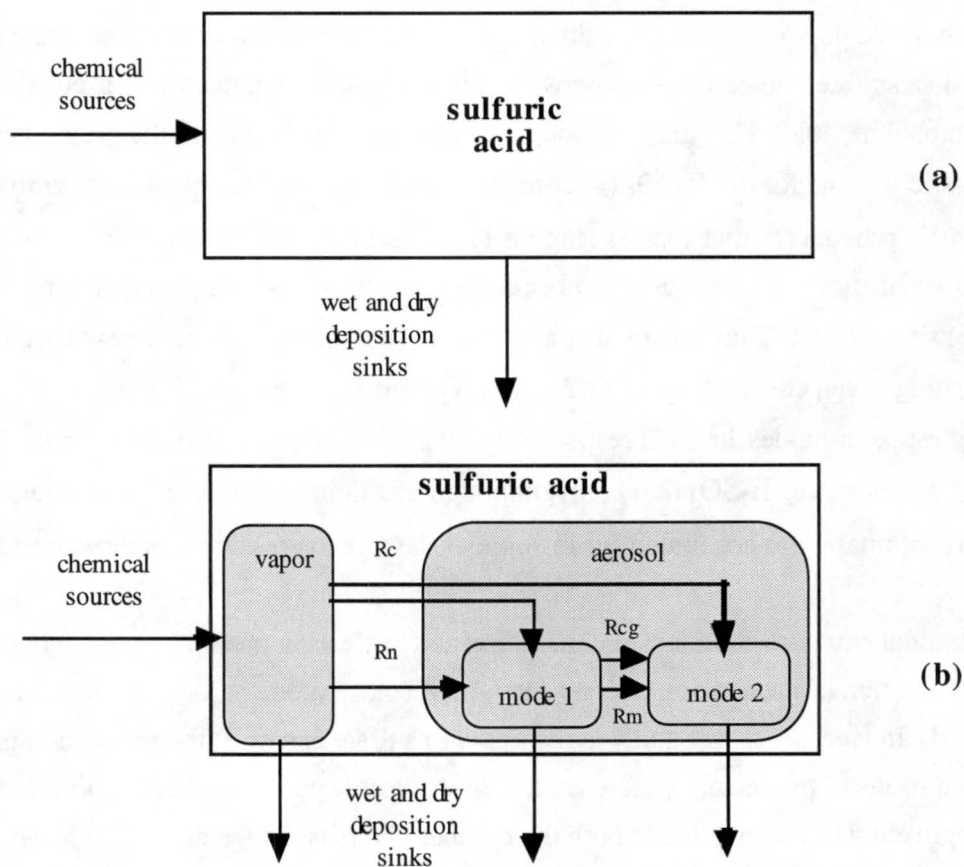


Figure 1. Schematic of treatment of the mass mixing ratio of H_2SO_4 .
 (a) Previous treatment, with diagnostic H_2SO_4 vapor; the total mass mixing ratio (vapor + particulate) is determined prognostically. Sources are chemical sources due to oxidation of SO_2 (Table 2); sinks are wet and dry deposition, applied to the total mass.
 (b) Present prognostic-vapor treatment, showing vapor / aerosol interaction pathways. Sources and sinks are unchanged from (a). R_c , condensation of vapor onto particles in both modes; R_n , nucleation of new particles into mode 1; R_{cg} , coagulation of mode 1 and mode 2 particles; R_m , merging of mode 1 particle number and mass into mode 2.

2.3.b *Microphysical processes in the aerosol model*

Most of the features of the two-moment aerosol model have been described in Youngblood and Kreidenweis (1994). The model is driven by the chemical source rate of H_2SO_4 (g) and includes parameterized equations for binary nucleation of sulfuric acid particles from the vapor phase, condensational growth of each mode, and inter- and intra-modal coagulation. The two aerosol modes evolve largely independently, with time-varying mass mean particles sizes in each mode determined by the ratio M_i/N_i . The modes interact only through intermodal coagulation and through an occasional “merging” process which combines the two modes into one if they contain similar-sized particles. Details regarding the rate expressions, the parameterizations, and the integration schemes used are furnished in the Appendix.

Although the prognostic variables are restricted to sulfate mass and number concentrations, implicit ammonium, dust, and water fields are used when diagnosing particle diameter for purposes of computing size-dependent mass transfer rates (*e.g.*, the rate of condensation of H_2SO_4 (g) onto preexisting particles). This parameterization assumes an ammonium sulfate aerosol in equilibrium with ambient relative humidity (*RH*) over the oceans; over land, similar assumptions apply, except that 30% by mass of insoluble species (silicate) is assumed. The effects of these assumptions are to somewhat increase the rates of sulfuric acid vapor scavenging and thereby suppress atmospheric levels of vapor-phase sulfuric acid.

The addition of particulate mass via the aqueous transformation of SO_2 is assumed to increase only the mass of mode 2 particles over the chemistry-aerosol coupling timestep. The rationale behind this treatment is that the larger mode 2 particles are the likely cloud condensation nuclei (CCN), and thus would receive this additional sulfate mass during a cloud cycle. However, since the aqueous conversion as modeled here proceeds throughout the atmosphere, regardless of the existence of CCN or clouds, it is possible to encounter conditions for which no mode 2 particles are present to receive this mass. To handle such situations, particle number is created if there are no particles preexisting in mode 2 at the time of this aqueous-phase mass addition; the added number concentration is determined by dividing the aqueous mass concentration to be added by the mass of a particle of 0.1 μm diameter. The model sensitivity to these assumptions and to the timestep on which the aqueous mass addition process occurs will be discussed in the Results section.

2.3.c Sequence of operations and timesteps used in the aerosol model

The flowchart of operations in the aerosol model is shown in Figure 2. As described in Section 2.2, the chemical source rates are updated each hour, yielding the source rate of H_2SO_4 (g) which is used to compute both nucleation and condensation rates. The check for the potential for nucleating new particles is based upon current environmental conditions (particularly RH and temperature, T), the vapor scavenging rates of preexisting particles in both phases, and, most importantly, the strength of the chemical source rate of condensable vapor. This determination is made every 300 s within the 1-hour outer loop, with condensed mass added over this timestep. If no nucleation is detected during the 1-hour outer timestep, then, upon completion of the condensational growth, intra- and inter-modal coagulation is carried out, followed by the addition of mass created via the aqueous-phase pathway to mode 2.

If nucleation of new particles occurs, the timestep used for the addition of new particle number concentration is that developed in the nucleation parameterization of Youngblood and Kreidenweis (1994). The timestep varies with environmental conditions and with the rate of production of H_2SO_4 (g). If it is longer than the overall 1-hour timestep, it is truncated to fit within that timestep. Nucleated particulate mass and number are added to mode 1, modifying the mean size of any particles which may have been preexisting in that mode.

The nucleation rate expression used by Youngblood and Kreidenweis (1994) in the development of their parameterization is the classical binary nucleation rate for sulfuric acid and water, modified for the presence of hydrates, as reported as a function of T and RH by Jaecker-Voirol and Mirabel (1989). For a given concentration of H_2SO_4 (g), the nucleation rate increases strongly with increasing RH and with decreasing T . This theoretical behavior, which has been verified to some extent by experiment, is reflected in the model results reported here, which tend to show that the nucleation pathway is favored in cold regions. Our results with respect to the competition between nucleation and condensation for sulfuric acid vapor in the atmosphere are therefore rather specific to this choice of nucleation rate expression, and it must be noted that these nucleation rates are subject to a great deal of uncertainty. Laboratory studies which have attempted to confirm the magnitudes of the rates and their dependence upon gas-phase species concentrations and temperature have generally found large discrepancies between theory and experiments

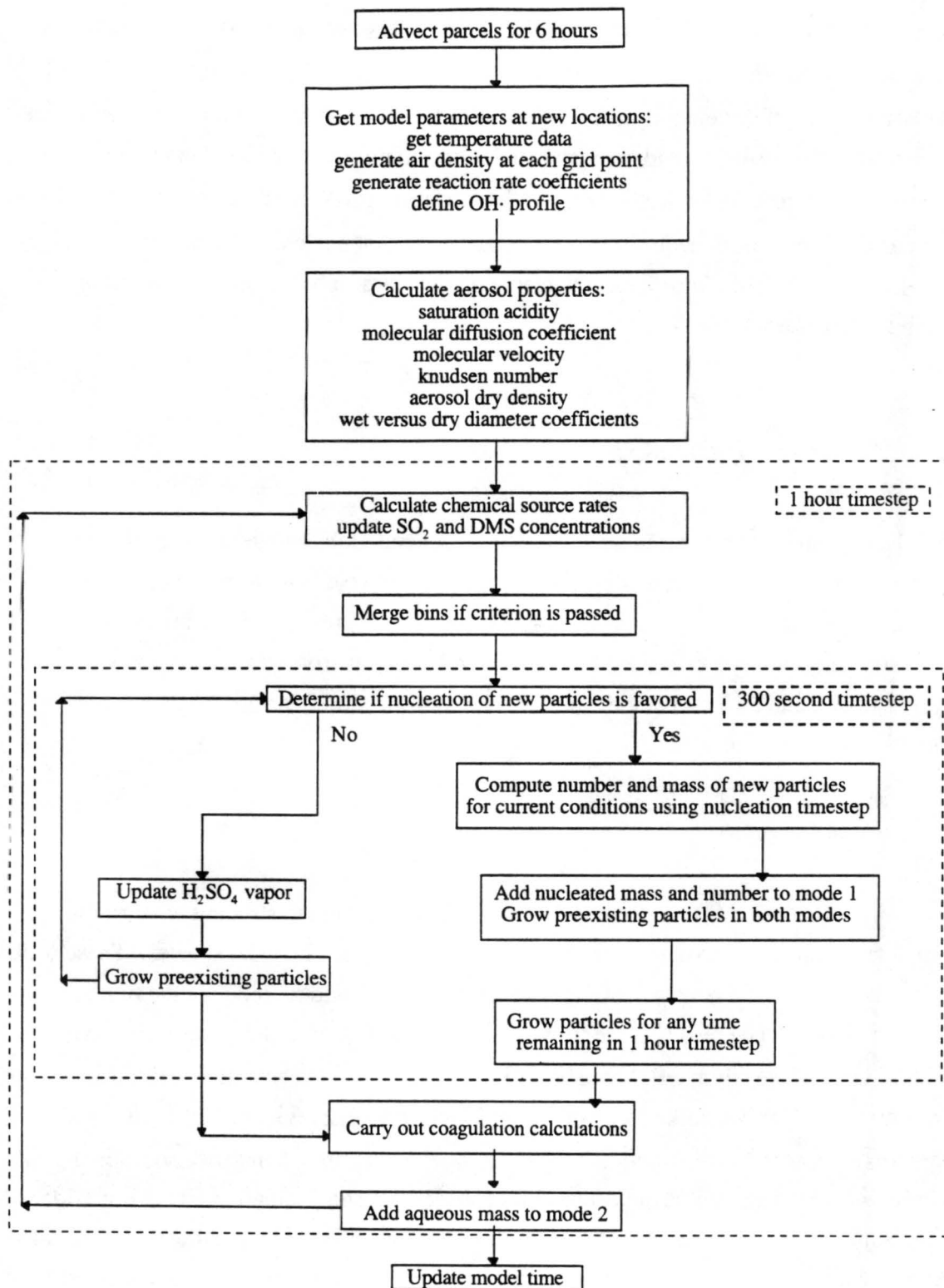


Figure 2. Flowchart of operations in the aerosol microphysics model.

(e.g., Wyslouzil *et al.*, 1991; Raes *et al.*, 1992). Recent observations of new particle production in the atmosphere under polluted-type conditions (Weber *et al.*, 1995) have in fact found a lack of correlation with the theoretically-important parameters, suggesting that species other than sulfuric acid are responsible for initiating nucleation. On the other hand, some observations (Clarke, 1992) suggest that ultrafine particles (diameter, D_p , < 0.01 μm) consist largely of unneutralized sulfuric acid, and that nucleation occurs in cold (high-altitude) regions of the atmosphere. Nucleation in the atmosphere is clearly an area in which further study is needed.

3. Results: Base cases

This Section presents and discusses results from several global model runs, performed with and without the aerosol model. Steady-state model results for July are presented; extensions to other seasons and to an annual cycle will be presented in future work. The chemistry-only runs are discussed first, followed by results from the aerosol model at two levels (surface and 355 mb) in the atmosphere. Aerosol-model sensitivity runs are described in Section 5.

3.1 Chemistry-only

The first simulations were performed using only gas-phase chemistry and were run for a complete annual cycle, to determine steady state fields for all chemical species. These were used to both verify the behavior of the new coupled model and to initialize the runs which included aerosol. The resulting monthly-averaged H_2SO_4 (total), SO_2 (total) and DMS fields at the surface ($\sigma = 1$) are shown in Figure 3. As expected, the peak mass mixing ratios at the surface are collocated with strong surface source regions. For H_2SO_4 and SO_2 these are in eastern North America, eastern Europe, and eastern Asia, with additional peaks near biomass burning regions in central South American and southern Africa. For DMS, ocean sources dominate, particularly near the strong upwelling region in the western Indian Ocean. These results were compared to results reported by Eddleman (pers. commun.) and found to be consistent with previous predictions using the model; the predictions are compared with a few selected observations in Section 3.2.

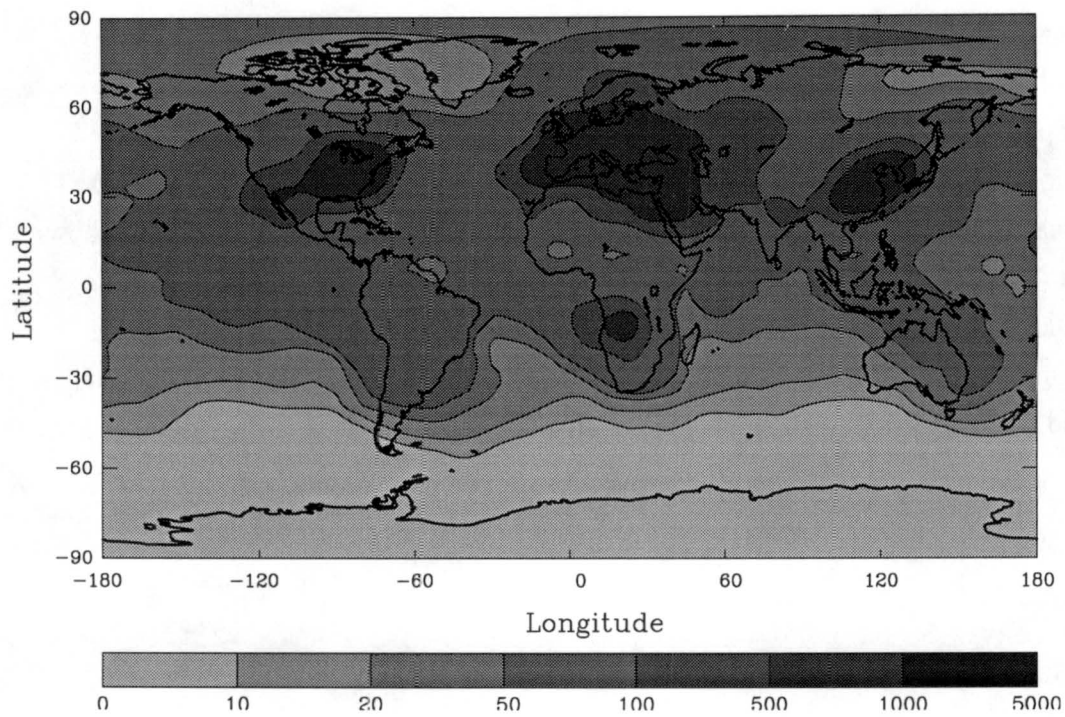


Figure 3a. Steady state H_2SO_4 [pptv] at the surface from chemistry-only simulation.

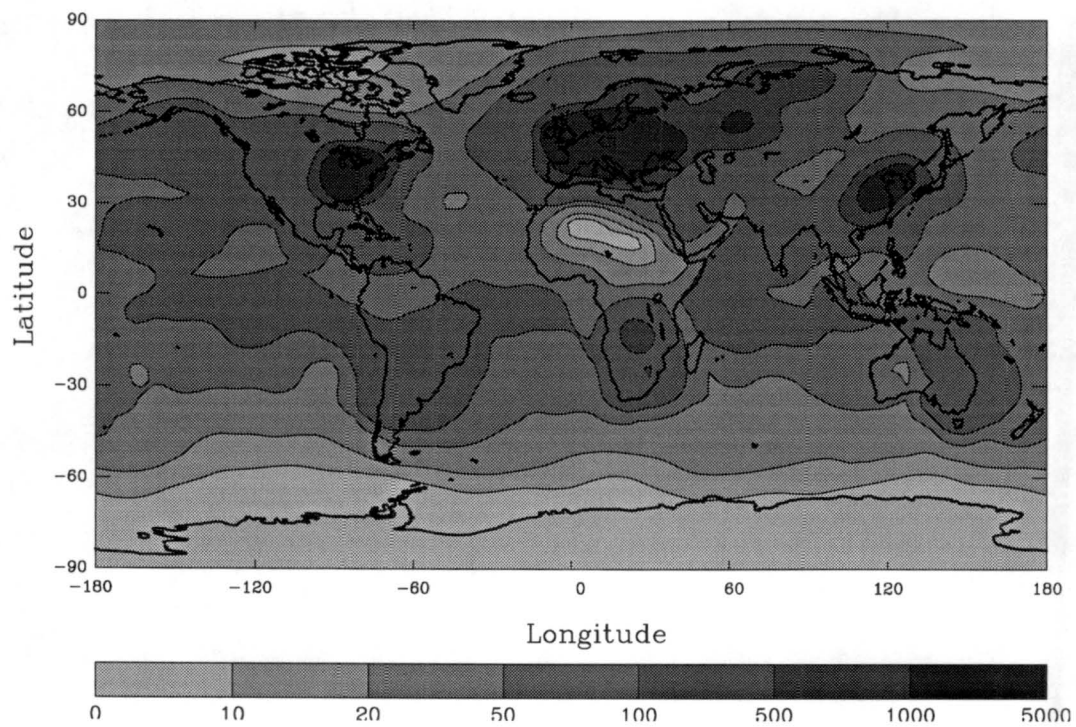


Figure 3b. Steady state SO_2 [pptv] at the surface from chemistry-only simulation.

Erickson *et al.* (1991) diagnosed particle number concentrations from a similar GRANTOUR run by dividing the steady state H_2SO_4 mass distribution into $0.1 \mu\text{m}$ - diameter particles. The diagnosed number concentrations were then compared with observations of CCN number concentrations. Applying this method to our steady state surface mass concentrations of sulfate (Figure 3a) yields the number concentrations shown in Figure 4. As expected, high number concentrations coincide with high sulfate mass loadings and are in regions of high sulfur gas source rates. Subsequent predictions of aerosol number concentrations, from the global model coupled to the aerosol model, will be compared with the distribution shown in Figure 4.

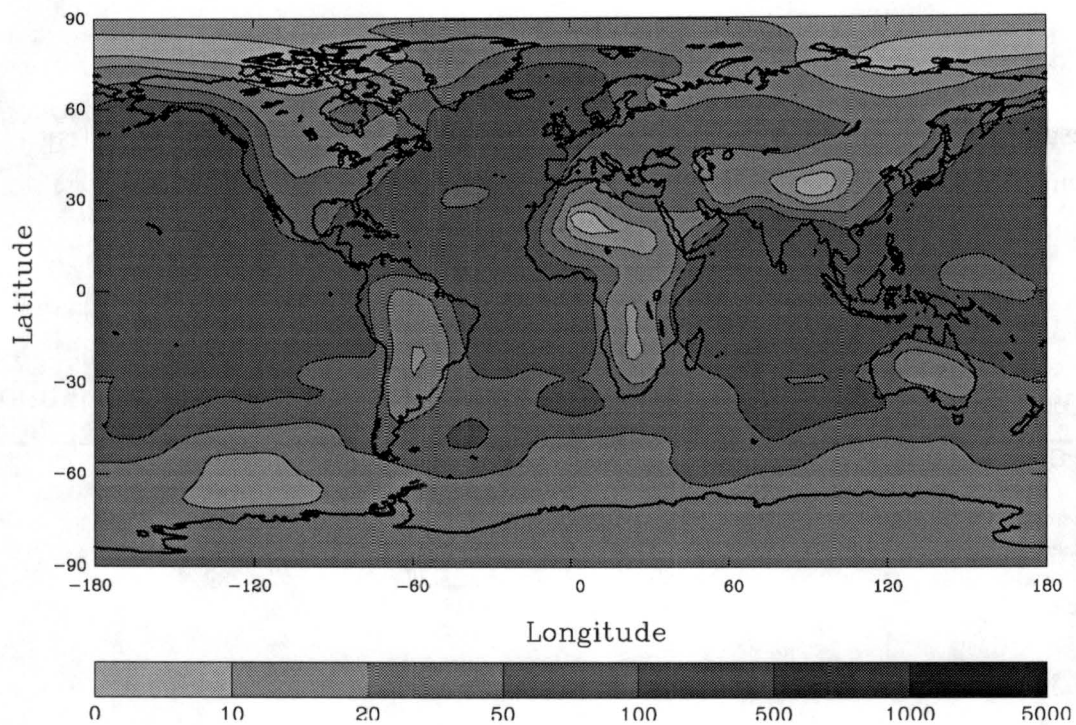


Figure 3c. Steady state DMS [pptv] at the surface from chemistry-only simulation.

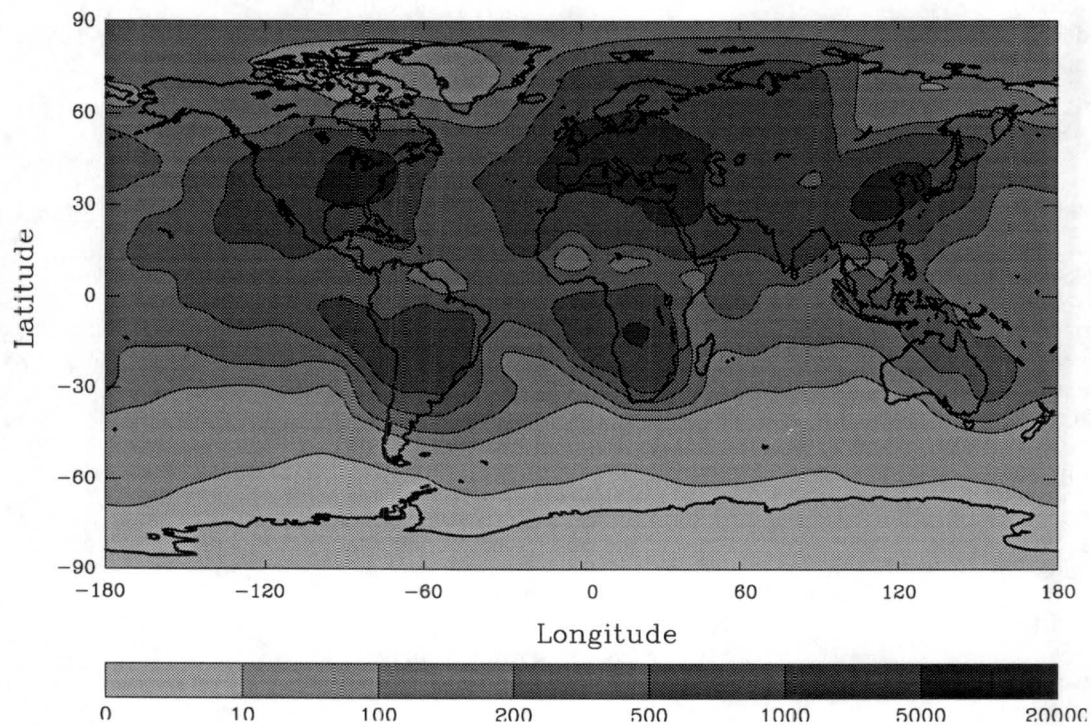


Figure 4. Particle number concentration [cm^{-3}] diagnosed from steady state H_2SO_4 chemistry-only results.

3.2. Comparison with observations

The results from the chemistry-only simulation were compared with data from numerous locations. Measurements and model results of DMS, SO₂ and non sea-salt sulfate concentrations are shown in Tables 3a, 3b, and 3c, respectively.

Table 3a. Comparison of DMS observations and model results.

Location	Latitude	Longitude	Reference	Observation (pptv)	Model Result (pptv)
Cape Grim	41 S	145 E	Ayers <i>et al.</i> , 1991	20	106
Amsterdam Island	38 S	77 E	Nguyen <i>et al.</i> , 1990	20 - 60	19
Equatorial Pacific	0	150 E - 150 W	Andreae <i>et al.</i> , 1985	47 - 289	98 - 265

Table 3b. Comparison of SO₂ observations and model results.

Location	Latitude	Longitude	Reference	Observation (pptv)	Model Result (pptv)
Lightship Charlie	52 N	35 W	Levy <i>et al.</i> , 1990	17	116
Southern Sweden	58 - 62 N	12 - 17 E	Schaug <i>et al.</i> , 1987	800	970 - 2362
Ohio River Valley	40 - 43 N	78 - 83 W	Shaw and Paur, 1983	5300	1953 - 2415

Table 3c. Comparison of H₂SO₄ observations and model results.

Location	Latitude	Longitude	Reference	Observation (pptv)	Model Result (pptv)
Cape Grim	41 S	145 E	Ayers <i>et al.</i> , 1991	5	42
Mace Head	53 N	8 W	Savoie <i>et al.</i> , 1989	450	1040
Bermuda	32 N	65 W	Savoie <i>et al.</i> , 1989	500	357
Tenerife	28 N	15 W	Savoie <i>et al.</i> , 1989	425	637
Barbados	13 N	60 W	Savoie <i>et al.</i> , 1989	275	136
Sptizbergen	79 N	12 E	Heintzenberg <i>et al.</i> , 1991	100	195
Lake Baikal	55 N	109 E	Pastukhov, 1991	100	114
Oahu	20 N	158 W	Savoie and Prospero, 1989	95	143
Fanning Island	3 N	160 W	Savoie and Prospero, 1989	170	96
Norfolk Island	30 S	168 E	Savoie and Prospero, 1989	18	82
Mawson	68 S	61 E	Savoie <i>et al.</i> , 1992	3	1
Southern Sweden	58 - 62 N	12 - 17 E	Schaug <i>et al.</i> , 1987	600	921 - 2022
Ohio River Valley	40 - 43 N	78 - 83 W	Shaw and Paur, 1983	2900	2190 - 2659

3.3. Coupled chemistry and two-moment aerosol model

Perpetual July meteorological conditions were used to examine the behavior of the aerosol model. The aerosol species were initiated by partitioning 90% of the H_2SO_4 mass, from the chemistry-only simulation, into 0.1 μm -diameter particles in mode 2; zeroing mode 1 aerosol species; and leaving 10% of the H_2SO_4 mass in the vapor phase. The initial conditions do not affect the steady state results shown here, but would have a large impact in a transient study. The simulation was run to steady state, as determined from the time series of the globally-summed species concentrations, by repeating seven July monthly cycles, and the last month was diagnosed for monthly mean values of the aerosol species. All steady-state gas-phase species distributions (except H_2SO_4 (g)) were unaffected by the addition of the aerosol model to the simulation.

3.3.a Surface : Steady-state monthly averages

As discussed in Section 2.3.a, the total sulfate mass concentrations predicted in the chemistry-only simulation are not affected by the inclusion of the microphysical aerosol model. The main difference is that in the run with the aerosol model, most of the sulfate mass is in the aerosol phase (Figure 5b), leaving only a few pptv in the vapor phase (Figure 5a). The predicted monthly mean concentrations of H_2SO_4 (g) (pptv) shown in Figure 5a indicate a maximum surface value of about 2.5 pptv, with many regions, particularly in the southern hemisphere and in the Arctic circle, significantly below 0.1 pptv. Measurements of ambient H_2SO_4 (g) are a fairly recent innovation (Eisele and Tanner, 1993) and few estimates of its distribution in the atmosphere exist. Eisele and Tanner (1993) report values of 0.04 - 0.4 pptv from their measurements made of a clean oceanic air mass at the Cheeka Peak Research Station. Estimates of surface vapor concentrations of a few pptv, as in Figure 5a, are probably not unreasonable.

Further explanation for the results in Fig. 5a considers the balances of sources and sinks leading to this steady-state result. H_2SO_4 (g) is produced via gas-phase reactions of SO_2 with $\text{OH}\cdot$, and the steady-state distribution of SO_2 is substantially lower in the Southern Hemisphere due to the weaker sources (Fig. 3b). Photochemistry is also less intense in the Southern (winter) Hemisphere. These predicted steady-state vapor values are largely controlled by the strength of this oxidation source, by the temperature dependence of the sulfuric acid vapor pressure used in our model (Ayers *et al.*, 1980), and by the

condensational growth rate expression. The concentrations approximate steady state values and may be thought of as the vapor concentrations required to support rates of nucleation and condensational growth which, together with transport and deposition, balance sulfuric acid vapor production. In the high source regions over industrialized countries the steady-state $\text{H}_2\text{SO}_4(g)$ is higher for the following reason. Since new particle formation (nucleation) is small, and does not remove much mass in any case, the high $\text{H}_2\text{SO}_4(g)$ source rates must be balanced by removal through transport or condensation onto existing particles. The condensation rate varies directly with the vapor concentration, so the vapor concentration builds until the condensation rate is sufficiently high to balance the chemical source.

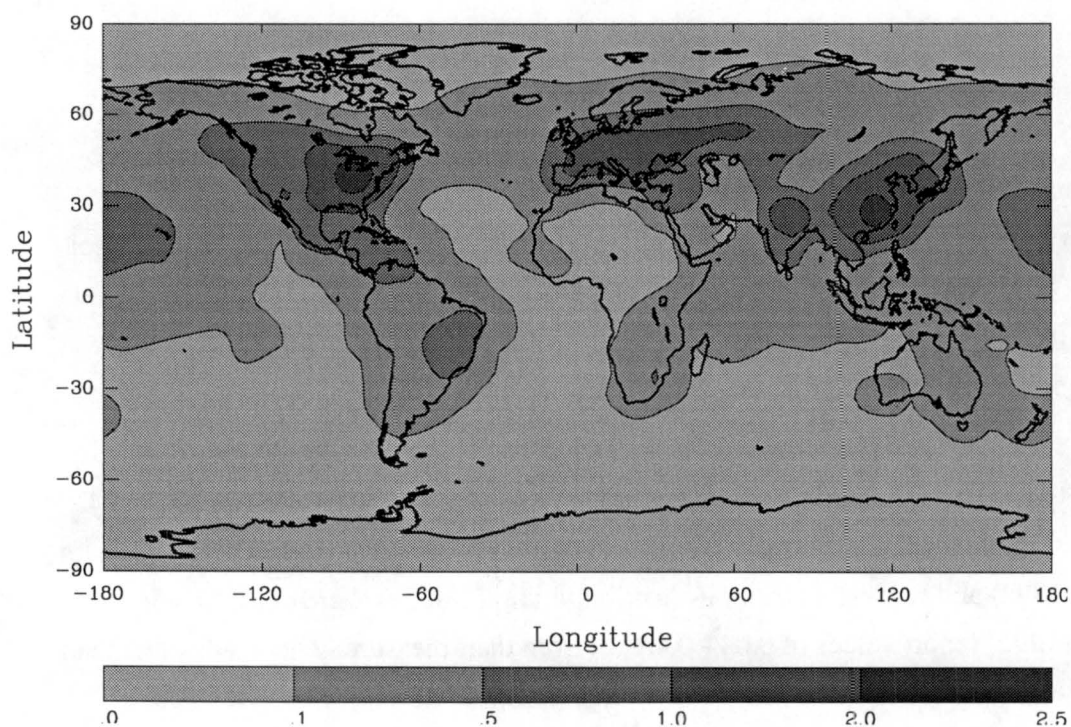


Figure 5a. H_2SO_4 (vapor) [pptv] at the surface from the coupled chemistry-aerosol simulation.

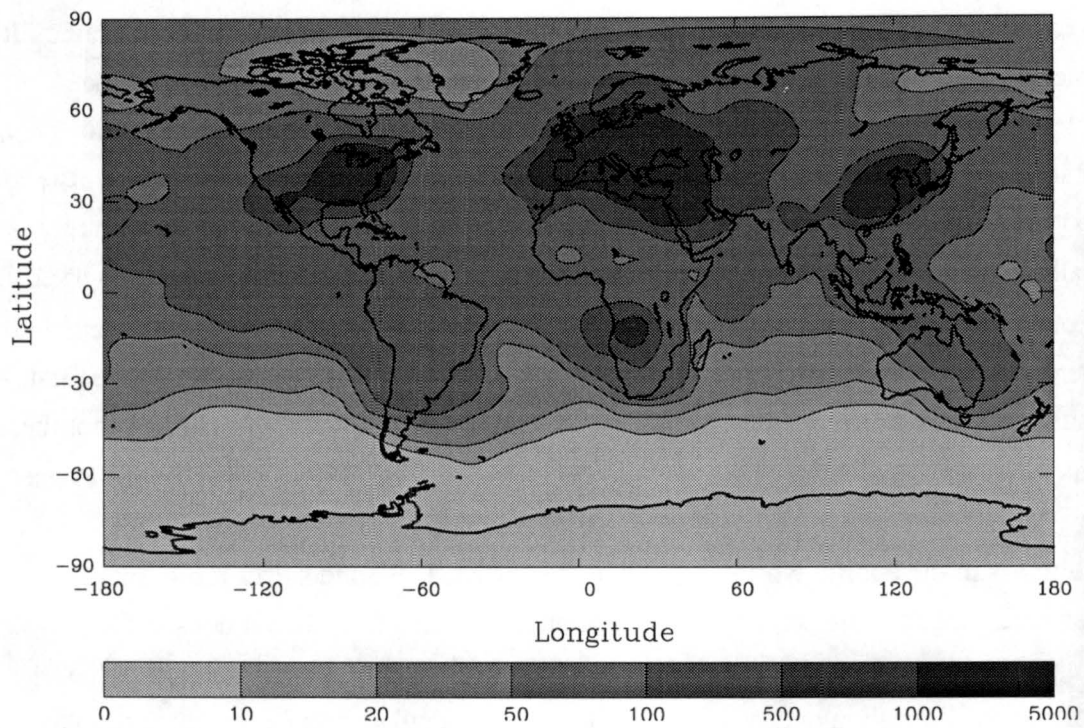


Figure 5b. H_2SO_4 (aerosol) [pptv] at the surface from the coupled chemistry-aerosol simulation.

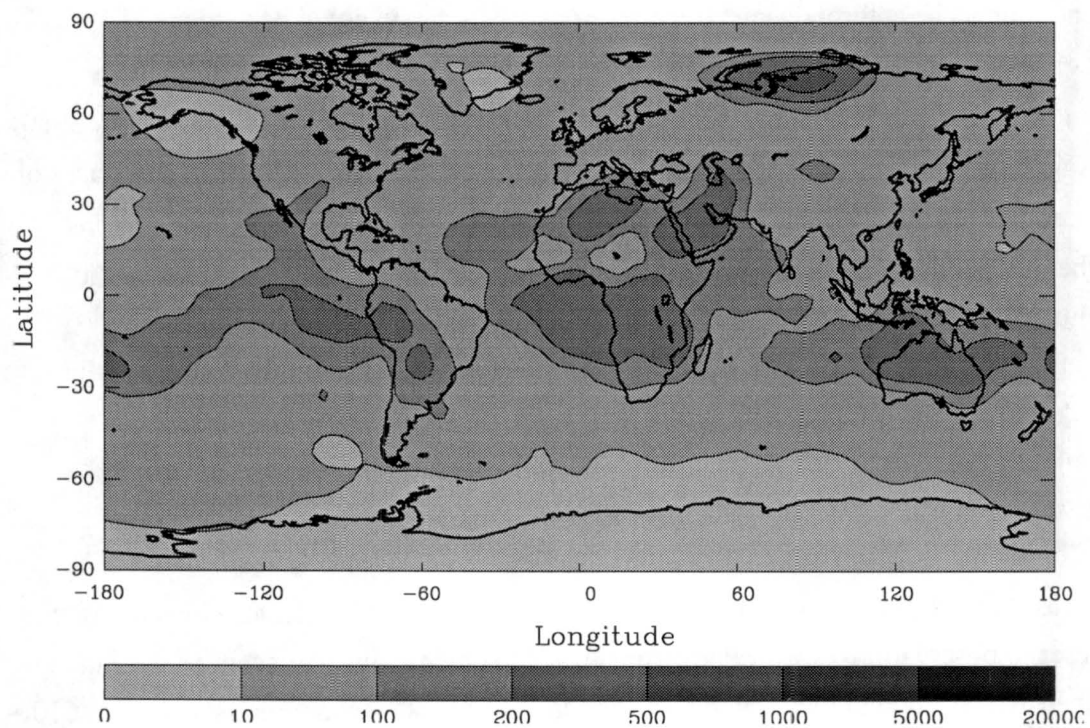


Figure 5c. Total aerosol number concentration [cm^{-3}] at the surface from the coupled chemistry-aerosol simulation.

The total surface number concentration (mode 1 + mode 2) (cm^{-3}) is shown in Figure 5c. It is immediately apparent that this Figure bears little resemblance to Fig. 4, and that the predicted continental number concentrations, particularly over the high anthropogenic sulfur source regions in North America, Europe, and Asia, are unreasonably low, on the order of $10 - 100 \text{ cm}^{-3}$. Observations of continental aerosol number concentrations are generally on the order of 1000 cm^{-3} (d'Almeida *et al.*, 1991), with higher values observed on an occasional basis and near source regions such as power plant plumes. The predicted number concentrations over industrialized regions are low for a number of reasons. First, only sulfur species were considered, and it is known that in many regions sulfur is not the primary chemical constituent of the aerosol mode (Malm *et al.*, 1994; Novakov and Penner, 1993). For example, organic carbon compounds make up large fractions of the fine particle mass in the Pacific Northwest and in the eastern U.S., and sulfur represents smaller percentages of the aerosol mass in the entire western U.S. than it does in the eastern parts of the country. It stands to reason that exclusion of a large fraction of the aerosol mass will result in underestimates of the total particulate number concentration as well. Second, in continental regions, direct emissions of particulate matter from sources such as combustion and windblown dust contribute strongly to the aerosol number concentration. The anthropogenic SO_2 emissions are in fact likely to be associated with direct emissions of particulate matter such as fly-ash and soot, which contribute both aerosol mass and number to the atmosphere. Observations (*e.g.*, Heggs and Hobbs, 1980) have suggested that SO_2 is efficiently and catalytically oxidized to sulfate on the surfaces of such particles. If this were the dominant mechanism for SO_2 oxidation in such regions, then the number concentrations of sulfur-bearing particles would be determined by the magnitudes of the direct particle emissions, and not by the microphysical processes represented in our model. Third, the rate of homogeneous nucleation over much of the land regions in the Northern Hemisphere is likely to be rather low in this model run, compared to an annual average, since July surface temperatures are warm, favoring condensation over homogeneous nucleation.

In contrast to the situation over land, the oceanic aerosol number concentrations in Fig. 5c are closer to observations, with values from $10 - 200 \text{ cm}^{-3}$ predicted, except near Antarctica (less than 10 cm^{-3} , due to the very low sources in July); most ocean regions are at least $10 - 50 \text{ cm}^{-3}$. While these values are still somewhat lower than those generally accepted, even for the non-sea-salt fraction of the aerosol (*e.g.*, Fitzgerald, 1991), it is interesting to observe that the better agreement in ocean regions suggests that the impact of localized

surface sources of aerosol number are not as important in shaping observed aerosol concentrations as they appear to be over land. This is consistent with the idea that sea salt, while a large fraction of the marine aerosol mass, does not contribute substantially to aerosol number concentrations in most circumstances. It should also be noted, however, that episodic, long-range transport of continental aerosol plumes does occur over ocean regions (Arimoto *et al.*, 1992; Hoppel *et al.*, 1990; Jensen *et al.*, 1996), and that these do substantially impact the marine aerosol. The model presented here cannot capture such events.

In summary, then, based upon the discussion above, we suggest that the lack of agreement between Figure 5c and surface observations of aerosol number concentrations is evidence of the importance of surface sources in controlling aerosol number concentrations, particularly over the continents. Homogeneous nucleation of sulfate, as parameterized here, is clearly not occurring everywhere at the surface to an extent appreciable enough to produce expected aerosol number concentrations. Three possible exceptions to this observation are the number peak over southern Africa (500 cm^{-3}), which is collocated with a sulfate mass peak and is in a region of strong SO_2 biomass burning sources, the number peak over northern Asia ($> 800 \text{ cm}^{-3}$), which occurs near a large anthropogenic SO_2 source and in a relatively cold and convectively stable area, and the number peak (500 cm^{-3}) which occurs over northwest Australia and is collocated with SO_2 biomass burning sources. Nucleation of new particle number is probably occurring to an appreciable extent near the surface in all three of those regions.

An additional observation from Fig. 5c is that, except for the three examples noted above, those regions with higher predicted number concentrations do not appear to coincide either with regions of strongest condensable vapor source rate (as deduced from Fig. 3b) or with regions of high sulfate aerosol mass loading (Fig. 5b). On the contrary, some of the highest predicted surface number concentrations are found over Saudi Arabia and northern Africa, where there are no appreciable sources of $\text{H}_2\text{SO}_4 (g)$ near the surface. The probable reason for the lack of coherence between high vapor source regions at the surface and high surface number concentrations is that nucleation is inhibited in regions with high mass loadings and large aerosol surface areas because the existing aerosol takes up much of the vapor and leaves little for producing new particles, as discussed above. Therefore, the existence of most of the number concentration peaks in Fig. 5c must be due to other processes, which are likely to include transport of high N into the region. In Section 4, a

case study of the origin of the number peak over northern Africa will be presented, demonstrating that such transport does occur.

Finally, the monthly averaged mass mean diameters for each aerosol mode are shown in Figure 6. These figures show wet particle size, that is, they include the effects of local *RH*. The predicted values are somewhat higher than might be expected: most of the mode 1 sulfate diameters are between 0.1 - 0.3 micron, while most of the mode 2 diameters are substantially larger than 0.5 micron. This result is not unexpected in light of the underprediction of the aerosol number concentrations, which, together with the mass concentrations, determine D_p . Although not shown here, the number concentrations of particles in mode 2 are generally significantly smaller than those in mode 1, so that while the mode 2 particles are unrealistically large, there are few of these cm^{-3} .

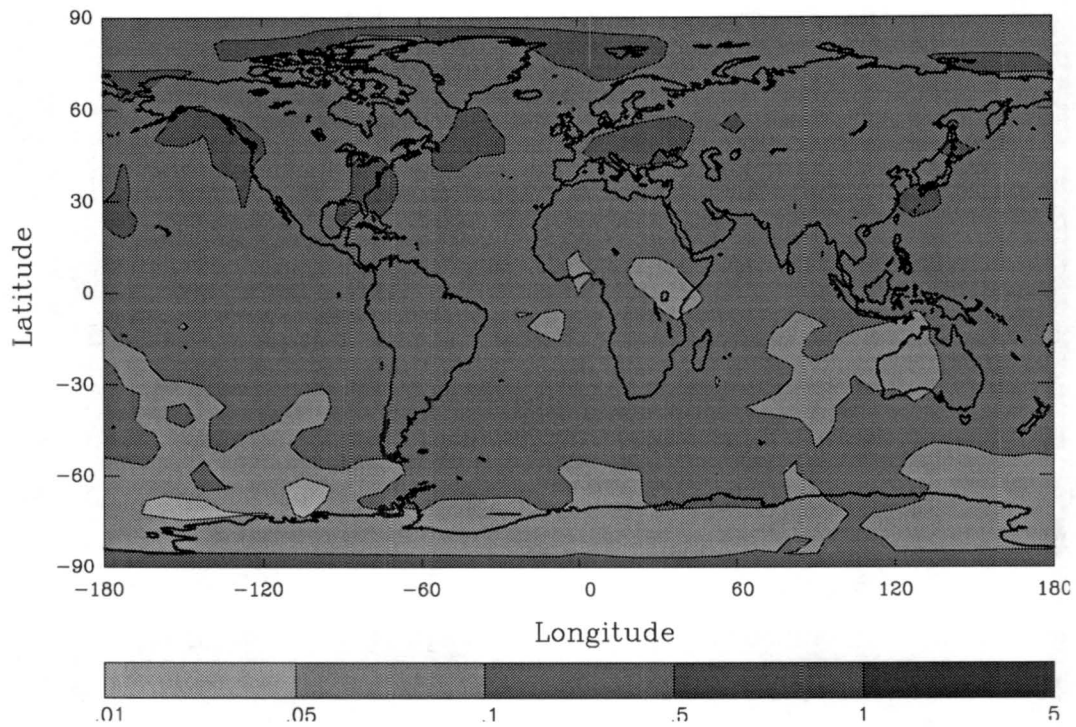


Figure 6a. Monthly averaged mode 1 mass mean diameter [μm] at the surface, including effects of local relative humidity.

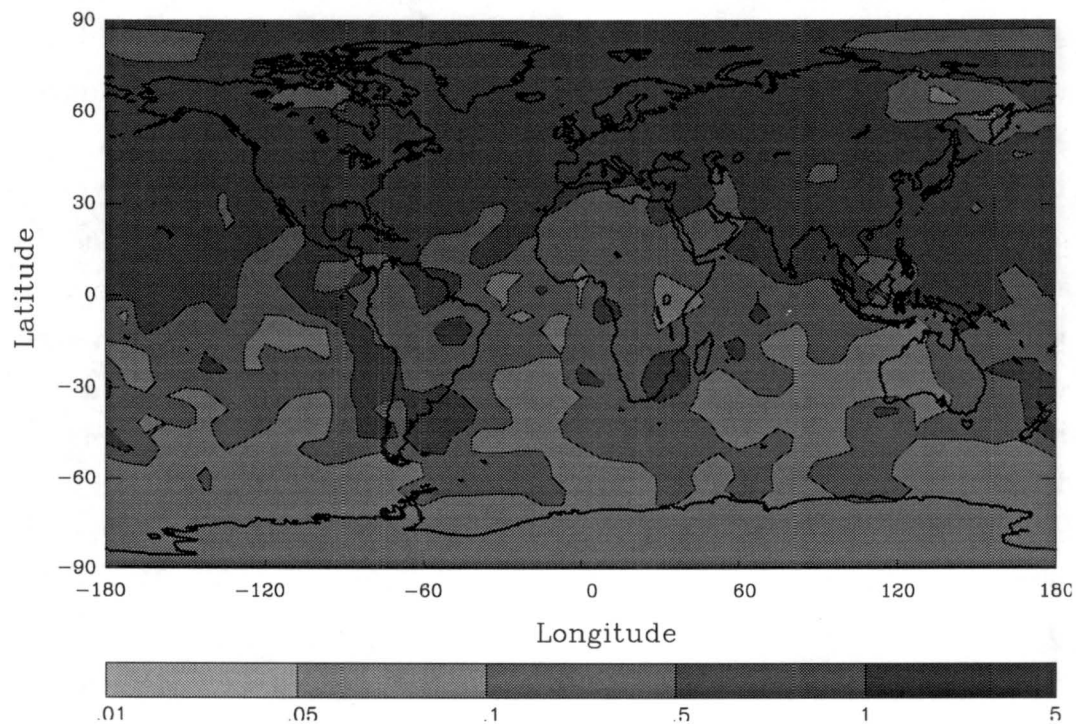


Figure 6b. Monthly averaged mode 2 mass mean diameter [μm] at the surface, including effects of local relative humidity.

3.3.b 355 mb : steady-state monthly averages

High number and low mass concentrations relative to those at the surface were predicted at a sigma level of 0.355 (P~355 mb) (Figure 7). This pressure level is at approximately 8 km in the troposphere. Low sulfuric acid vapor concentrations are expected at this altitude, both because the low temperatures lead to a very low saturation vapor pressure for H_2SO_4 and because the source of $\text{H}_2\text{SO}_4(g)$ is dependent upon volcanic inputs and on convective transport of other SO_2 emissions to these levels. Based on the location of the aerosol mass peaks (Fig. 7a) it appears that vertical transport of anthropogenic SO_2 emissions from the eastern U.S. and Europe does occur and leads to relatively high sulfate mass loadings over those regions, and indeed over most of Asia. Recall that the summertime is a region of convective thunderstorm activity over Europe and the eastern U.S., and strong convection associated with the summer monsoon over India. Although this convective transport is probably captured only crudely in the CCM1 transport fields, it does appear to have an effect on the coupled chemistry / aerosol model predictions.

At 355 mb, the lowest number concentrations (less than 100 cm^{-3}) are predicted in the $0^\circ - 30^\circ \text{ N}$. latitude band, and the highest (1000 cm^{-3} and greater) occur between 30° and 60° S . Observations of bands of high aerosol number concentrations are not inconsistent with observations (*e.g.*, Clarke, 1992), although Clarke found enhancements at 8 – 10.5 km in the $0^\circ - 5^\circ \text{ S}$. latitude band during an April transect from Darwin to Tokyo. Clarke (1992), among others, have suggested that transport of particle precursors (primarily SO_2) to the upper troposphere occurs in the ascending branches of the Hadley and Ferrel cells, and that low temperatures in the upper troposphere support the nucleation of new particles from the H_2SO_4 produced as the precursor gases are oxidized. Fig. 7b supports this theory in some respects: ascending air near 60° N . and 60° S . brings unreacted gases to the mid- and upper-troposphere, and oxidation and subsequent nucleation during the transit toward descending regions near 30° N . and 30° S . may be responsible for the relatively high predicted N in those bands. If this is true, then it is somewhat surprising that a similar phenomenon is not observed in the $0^\circ - 30^\circ \text{ N}$. and $0^\circ - 30^\circ \text{ S}$. bands, which might be expected to have analogous vertical air motions that would support similar aerosol phenomena. However, rising air near the equator is also associated with low SO_2 sources and heavy precipitation, which removes not only aerosol and $\text{H}_2\text{SO}_4(g)$, but also the precursor SO_2 . Removal, in addition to warmer temperatures near the equator that do not favor nucleation, may explain the low N predicted in those regions.

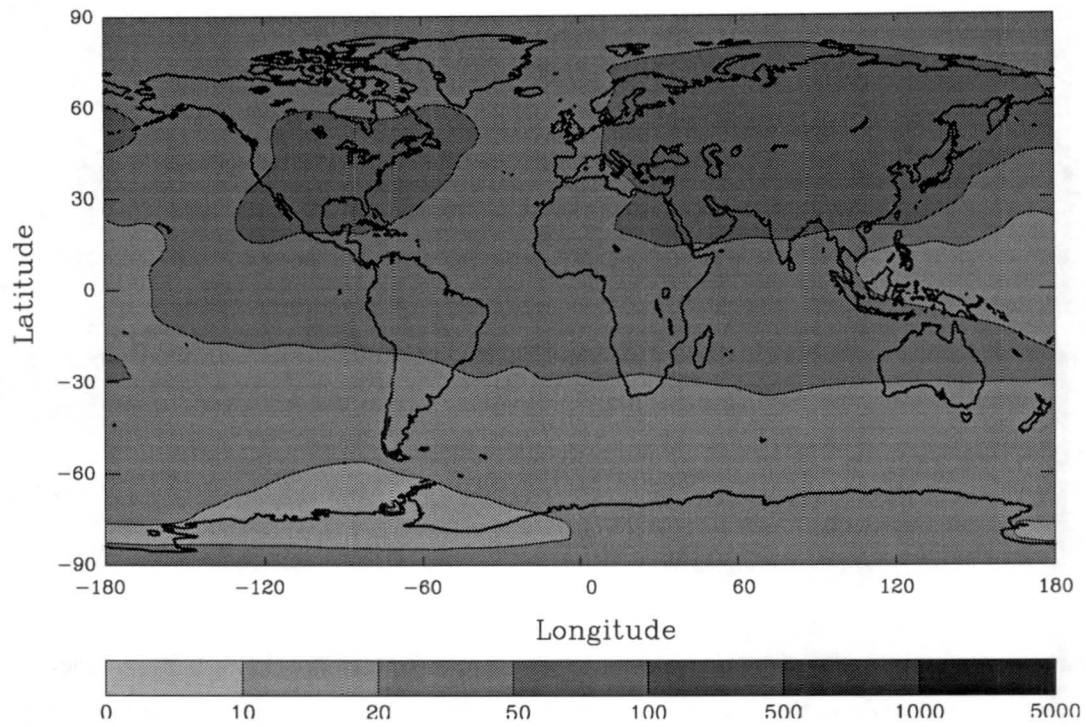


Figure 7a. H_2SO_4 (aerosol) [pptv] at ~355 mb from the coupled chemistry-aerosol simulation.

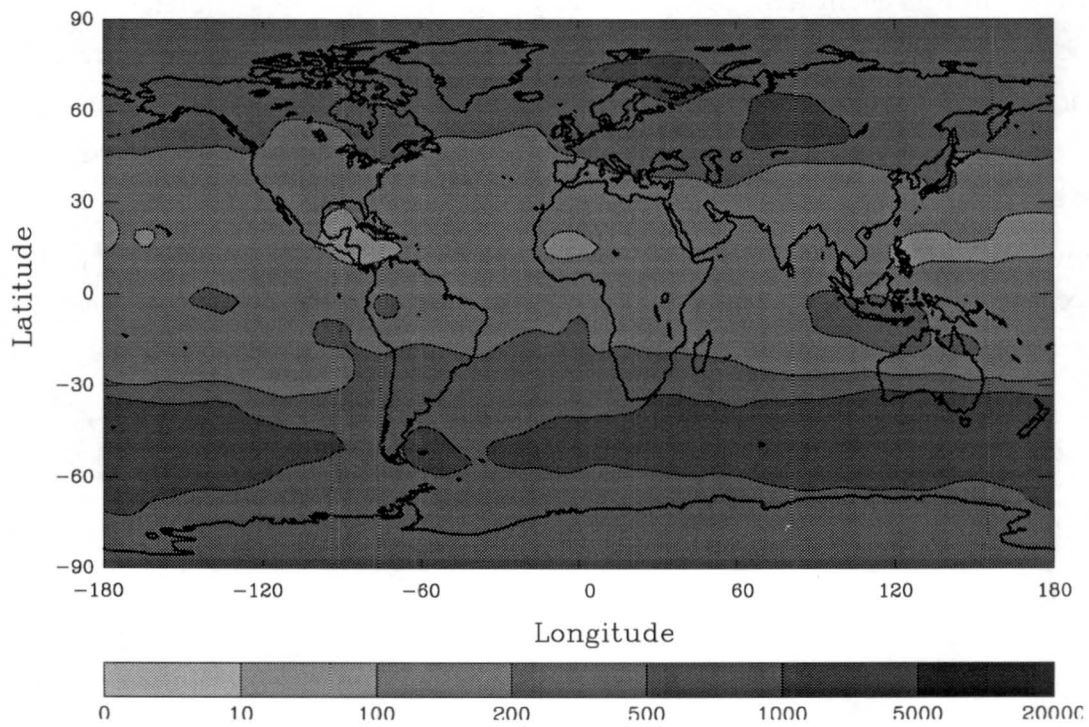


Figure 7b. Total aerosol number concentration [cm^{-3}] at ~355 mb from the coupled chemistry-aerosol simulation.

4. Analysis of aerosol transport to surface at 7.5° E., 28.9° N.

This Section presents a case study analyzing the processes controlling the predicted surface aerosol number concentrations near 7.5° E., 28.9° N., over northern Africa. This region was selected for study because of the relatively high predicted monthly-mean N (Fig. 5c), which is neither associated with any strong local sources, nor with a noticeable collocated peak in monthly-mean aerosol mass. Further, it occurs over a desert region, whose high temperatures and low RH are expected to suppress nucleation of new particles.

4.1 Time history of predicted values

To determine which modeled processes were responsible for the monthly-mean number concentration peak seen in this region, the time-dependent number concentration was first examined. Figure 8 shows the time history of the total number concentration at the CCM1 grid point closest to the center of the number peak (7.5° E., 28.9° N.). It is immediately seen that the high monthly-mean values are the result of averaging episodic high number concentrations with alternating low concentrations, with factors of 3 – 10 difference between the highs and lows. The time history of N appears to be periodic, and indeed, similar number peaks occur at the same time of the month in previous month's runs. The last number peak of the month is a particularly robust one, occurring at the same time in all of the previous 4 months' runs. This observation, together with the approximately 7-day period, strongly suggest synoptic scale-transport as one of the factors modulating N at the surface here. Since a perpetual July meteorology has been used, the similar peaks in repeated monthly cycles may point to a meteorological origin.

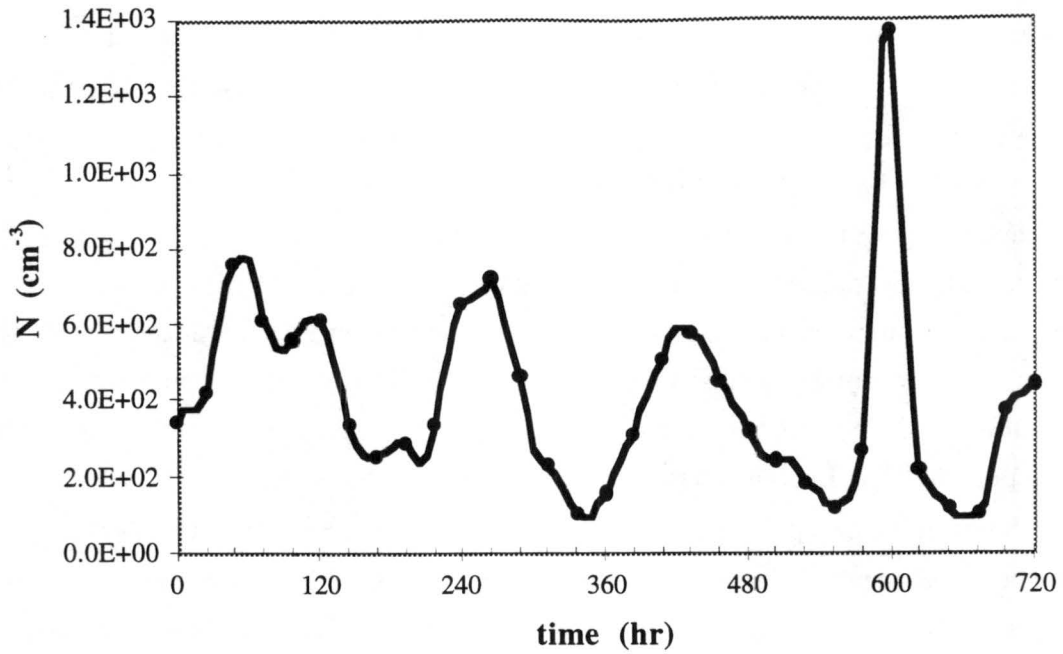


Figure 8. Time history of the total aerosol number concentration [cm^{-3}] at the surface grid point, 7.5° E, 28.9° N.

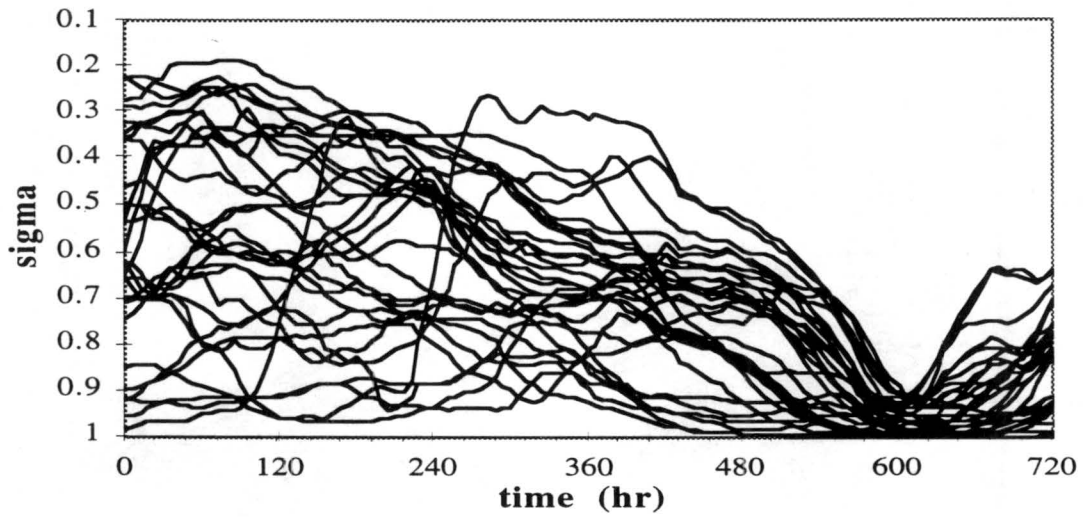


Figure 9a. Vertical trajectories of all parcels which contribute significantly to the grid point [7.5° E, 28.9° N] total aerosol number concentration at hour 600.

Figure 9a shows the time-dependent vertical position of all Lagrangian parcels which contribute to the aerosol number concentration at the grid point at 600 hr, the highest 6-hour average value of N observed at this location. At 600 hr, all of these parcels are located near the surface, which is a prerequisite for them to have a significant contribution to the grid point species values at $\sigma = 1$. Interestingly, many of these parcels have spent significant time prior to their arrival at the grid point at higher levels of the atmosphere ($\sigma < 0.5$); indeed, the trajectories suggest strong subsidence occurring in the grid point region. Similar migrations of parcels from low sigma value levels towards the surface also occur during other number peaks in this month, while this trend is absent for parcels contributing to the low number values. For example, Figure 9b shows the time-dependent vertical position of all Lagrangian parcels which contribute to the aerosol number concentration at the grid point at 342 hr, the *lowest* six-hour average value of N observed. While the parcels again are located near the surface at 342 hr, they have arrived from lower vertical levels (generally, $\sigma > 0.5$) than those in Fig. 9a. This suggests that some air masses which remain near the surface tend to have relatively low aerosol number concentrations, either because the nucleation source is weak near the surface or because wet and dry deposition processes are effective sinks for aerosol number and mass over several days' transport time.

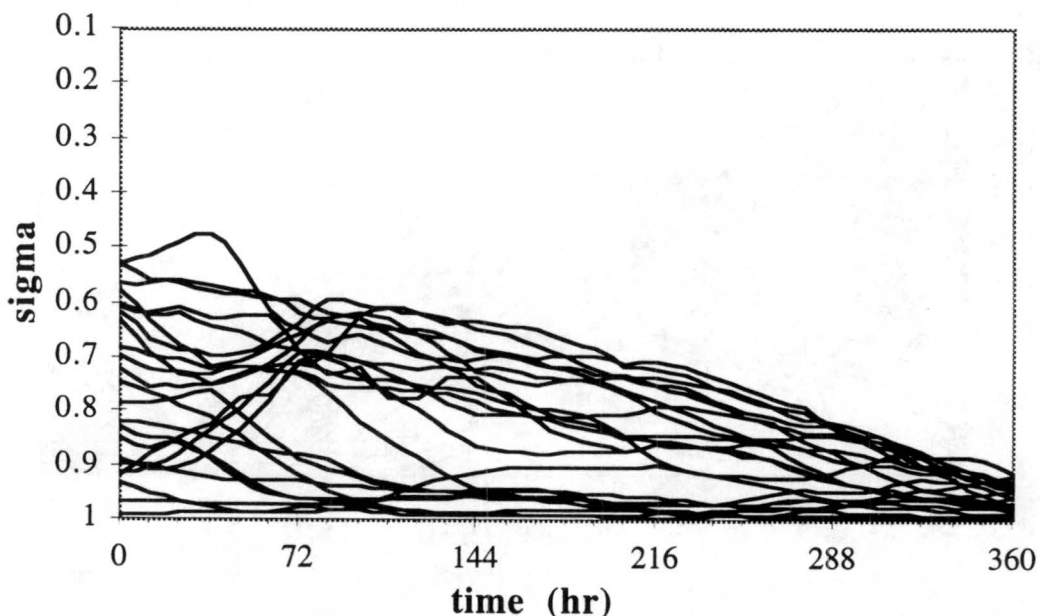


Figure 9b. Vertical trajectories of all parcels which contribute significantly to the grid point [7.5° E, 28.9° N] total aerosol number concentration at hour 342.

The contributions of such air masses to aerosol species values at an Eulerian grid point give rise to minima in aerosol number concentrations. In contrast, some air masses which are lifted to higher levels in the atmosphere can gain and retain relatively high aerosol number concentrations. The depletion of aerosol number at high altitude is slowed by the lack of effective sinks: dry deposition is active only for $0.9 \leq \sigma \leq 1.0$, so removal in convective precipitation or diffusional mixing are the only pathways. If the parcel does not encounter strong precipitation at these high altitudes, then most of the nucleated particles can remain in the parcel as it is transported, and if it is brought toward the surface, as occurs at 600 hr in Figure 9a, it contributes this high N to the diagnosed values at nearby grid points.

4.2 *Three-dimensional trajectory of a single parcel*

Of the parcels which contribute to the high value of N at the surface at 600 hr, one parcel accounts for 60% of the total number concentration at the grid point. This parcel is now analyzed in more detail, to support or refute the relationship between parcel position and number concentration postulated in the previous section. The latitude and longitude of the parcel are shown in Figure 10a; each tick mark represents a 1 day timestep.



Figure 10a. Trajectory of one parcel which contributes 60% to the grid point [7.5° E, 28.9° N] total number concentration at hour 600.

At the beginning of the month, the parcel is located near the surface over the mid-Atlantic Ocean. It first migrates northwest toward the east coast of Canada, is swept partway down the western Atlantic some distance off the coast of the U.S., and is then transported rather rapidly northeastward to the British Isles. It crosses eastern Europe, loops in the eastern Mediterranean, and then is caught in a northeasterly flow that brings it to the west coast of central Africa by the end of the month. This transport, however, is not occurring at one altitude (Fig. 10b). The parcel is located in the marine boundary layer during the initial migration toward North America, but is then rapidly lifted to a 300 mb level as it is transported across the Atlantic. The particle number concentration is quite low until the parcel reaches these higher altitudes (about 168 hr), at which time the number concentration rises rapidly. Later in the simulation (576 hr), when the parcel is again in the boundary layer, it loses aerosol number to deposition processes.

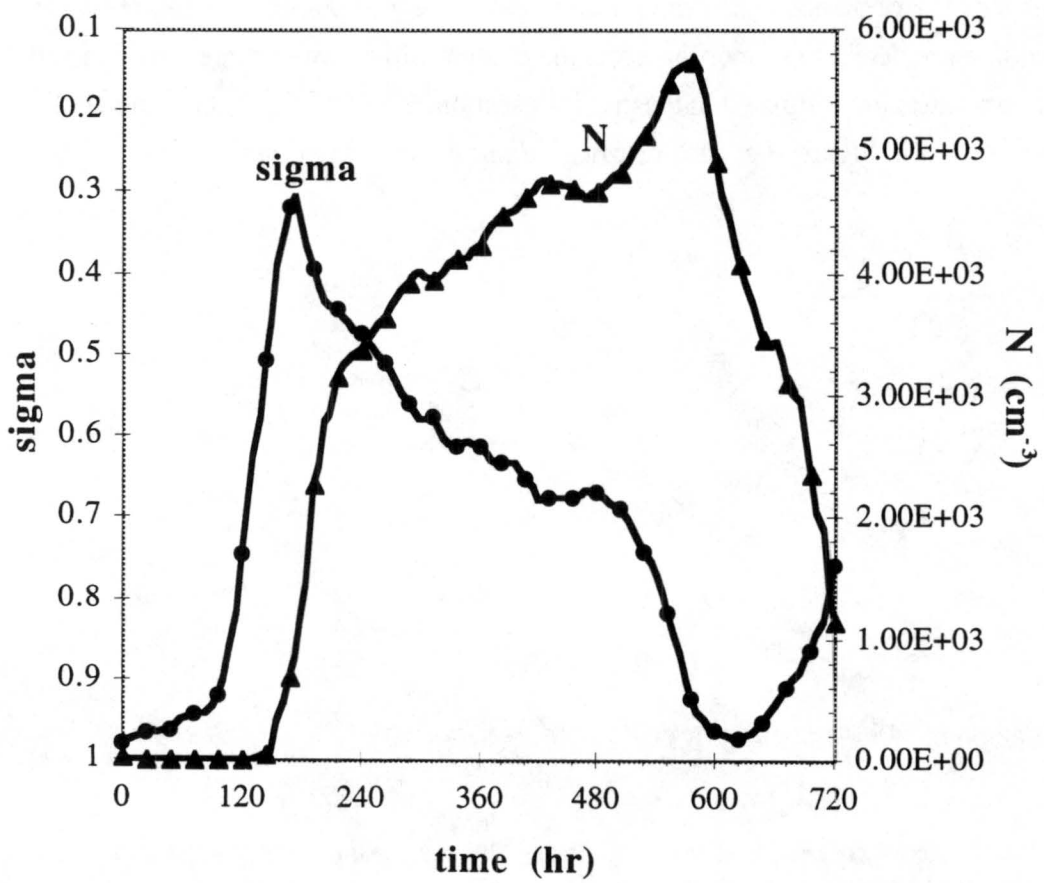


Figure 10b. Vertical trajectory and total aerosol number concentration for parcel shown in Figure 10a.

Interestingly, the aerosol mass mixing ratio (Fig. 10c) rises during the parcel's initial westward transport toward the North American continent, even though the number concentration is so low. This is consistent with the discussion of Figure 5, which showed that the model predicted low number concentration but high sulfate mass off the eastern coast of the U.S. The parcel picks up not only aerosol sulfate mass, but also SO_2 and $\text{H}_2\text{SO}_4(g)$ (Fig. 10c) from the plume off the eastern U.S. As the parcel is swept into the upward and southeasterly flow across the Atlantic, the concentrations of gas- and aerosol-phase sulfate and of SO_2 drop, possibly due to a precipitation sink. However, there is enough remaining SO_2 and $\text{H}_2\text{SO}_4(g)$ to support the formation of new particles at altitudes above 500 mb, where the cold temperatures favor nucleation. Conversion of SO_2 into $\text{H}_2\text{SO}_4(g)$, and then into aerosol mass, appears to continue until 408 hr, when the parcel is just above 700 mb and over the eastern Mediterranean region. At this point, it again increases its SO_2 and $\text{H}_2\text{SO}_4(g)$ mixing ratios, probably by picking up surface emissions that have been transported to the 700 mb layer. The number concentration (Figure 10b) also increases between hours 480 and 576. It is worth noting that, just prior to the time of the strong number peak at the grid point (600 hr), the parcel number concentration begins to drop, coincident with the parcel moving below the 900 mb level. This is the height below which dry deposition processes become significant, and indeed the effects of deposition are evident in all of the species mixing ratios shown in Figs. 10b and 10c.

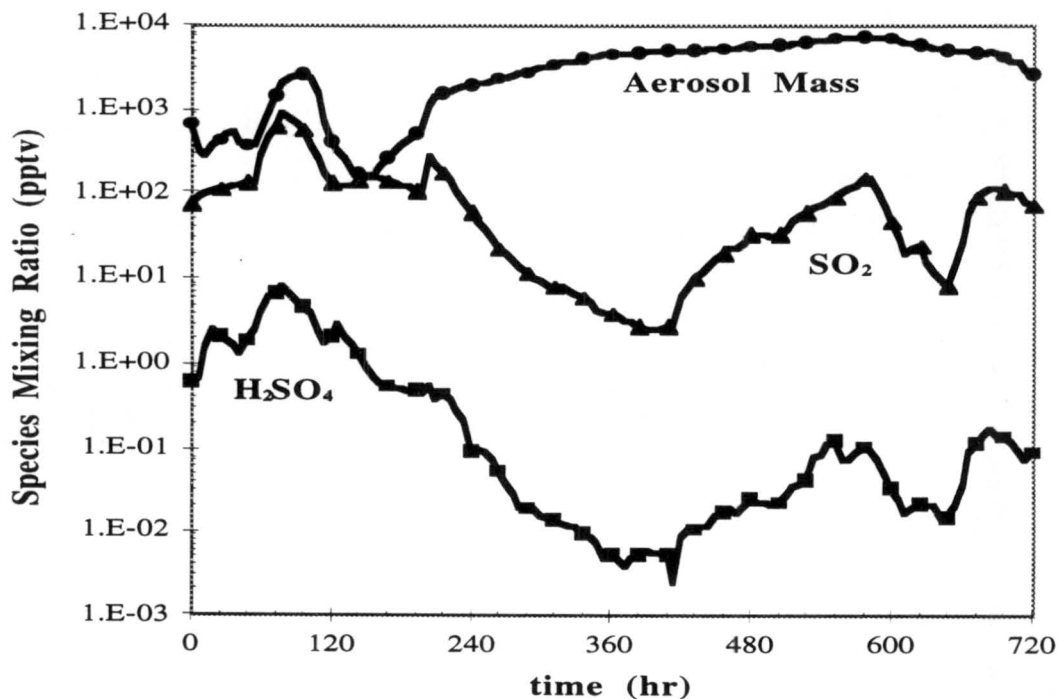


Figure 10c. Time history of mass mixing ratios for parcel shown in Figure 10a.

Finally, after 480 hr, the parcel descends over about a 5-day period from 700 mb toward the surface, where it contributes to the high N values at the 7.5° E., 28.9° N grid point at 600 hr. The synoptic-scale weather conditions must have been such that subsidence from aloft was favored at the grid point just before this peak occurred. The air masses thus sampled by the grid point had histories similar to that of the parcel just analyzed, resulting in a number concentration peak when the upper-level air reached the surface. In contrast, when low N are observed at the grid point, air masses from different, lower regions of the atmosphere are sampled; these air masses have not been lifted after receiving unreacted precursor gas emissions in the lowest levels, as the parcel analyzed here had, and thus had not supported new particle formation during their transport to the grid point area.

This case study represents just one of the 50,000 parcels for which such time histories were computed. Thus the conclusions reached here, while not refuting the hypothesis that new particle formation occurs in ascending air masses which contain unreacted precursors and which reach cold levels of the atmosphere, are not completely general either. Likewise, subsiding air masses will not always be associated with transport of high particle number concentrations toward the surface. However, this hypothesis appears to explain the model behavior which forms the number concentration peak over northern Africa. It is also evident from this analysis that the Lagrangian-parcel framework of GRANTOUR is very useful for investigating predicted phenomena using back trajectories; identifying source regions such long distances from the observation point would be much more difficult in an Eulerian model. On the other hand, investigating regional phenomena, such as relative highs and lows in predicted N , are more difficult to unravel in the parcel-model formulation, since to do so one must investigate the time histories of all parcels which contribute to the observed phenomenon. Clearly, both approaches have strengths and weaknesses.

5. *Sensitivity simulations*

5.1 *Alternate merging mechanism*

In the two-moment, two-mode approach, the most appropriate method of allowing the modes to interact is not well defined. One option is to allow the modes to remain independent throughout the simulation. However, condensational growth will certainly increase the mode 1 diameter, and it is possible that the mode 1 and mode 2 diameters will

become nearly equal in size. This is not desirable since, if nucleation occurs, the nucleated number and mass are added to mode 1, combining with the moments already carried in that mode; if the mean size of the preexisting mode 1 particles are too large, the nucleated particles will not be represented as small particles by this method. Also, the effect of carrying particles that are too large is to unrealistically enhance the condensation rate, suppressing sulfuric acid vapor buildup and suppressing nucleation of new particles. As described in the Appendix, the approach used here was to compute, at each hourly time step, the condensation rates onto each particle mode and onto a merged mode, and to merge the two modes into a redefined mode 2 if the summed condensation rates approximated the rate which would be computed for the merged mode.

An alternative method is to continuously merge a portion of the mode 1 particles into mode 2, with the amount of mass and number transferred depending upon the condensation rate onto mode 1 particles (see Appendix). This approximates the growth of the larger mode 1 particles into the mode 2 size range and results in a continuous transfer of particles from mode 1 to mode 2.

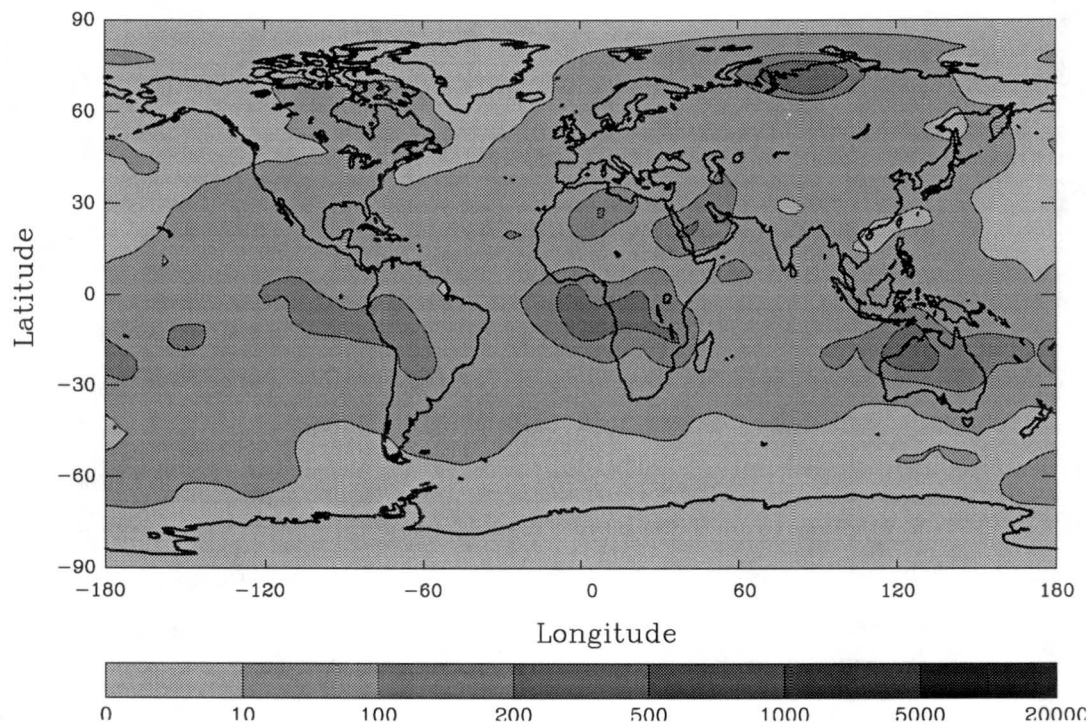


Figure 11. Total aerosol number concentration [cm^{-3}] at the surface for sensitivity study using the alternate merging mechanism.

To test this alternate approach, this sensitivity simulation was carried out in the same manner as the 'base case' model run discussed above. Seven months of perpetual July meteorology were again required for the case to reach steady state. The monthly average of the seventh month was used for this analysis. The resulting surface number concentrations are shown in Figure 11.

Although the condensation rates are changed with this approach, this method of merging modes did not substantially affect the gas-phase species of the total aerosol mass. Only total particle number concentration was significantly altered. As a result of the continuous transfer of mass and number to mode 2, more particles reside in mode 2, relative to the 'base' case run (Fig. 5c). The resulting increased aerosol surface area inhibits nucleation, thereby reducing the total number concentration of particles. The trends in total number concentration at the surface shown in Fig. 11 are similar to those in Fig. 5c, but the values are somewhat lower. Maximum values of N are reduced by about a factor of two. The global monthly mean tropospheric aerosol number concentrations are reduced by 43%.

5.2 *Alternate timesteps*

On the global scale, the transformation of SO_2 to particles via the aqueous pathway is the dominant source of sulfuric acid mass, so a strong sensitivity of the model results to the treatment of this pathway is not unexpected. A sensitivity test was performed to examine one aspect of the interaction between the aqueous-phase chemical pathway and the aerosol model.

The typical coupling timestep between the GRANTOUR gas-phase chemistry calculation and the aerosol microphysical calculations is 1 hour, as shown in Fig. 2. This gives frequent enough updates to the chemical source rates to allow accurate prediction of the onset of a nucleation burst, while using reasonable amounts of computer time. Increasing the chemistry timestep to 3 hours, so that the chemical source rates are updated every three hours, does not significantly affect the results. However, when both the chemical source rates and the aqueous mass addition to the aerosol are updated on 3 hour coupling timesteps, with coagulation and merging calculations performed at 1 hour timesteps, differences are found in surface N values over southern Africa, Europe and other locations (Fig. 12). The differences in the global monthly mean tropospheric aerosol number concentration, on the order of 1-10%, are primarily due to increases in N_2 , and indicate that

the effects on the aerosol model of the addition of the aqueous-pathway mass are quite sensitive to its coupling timestep.

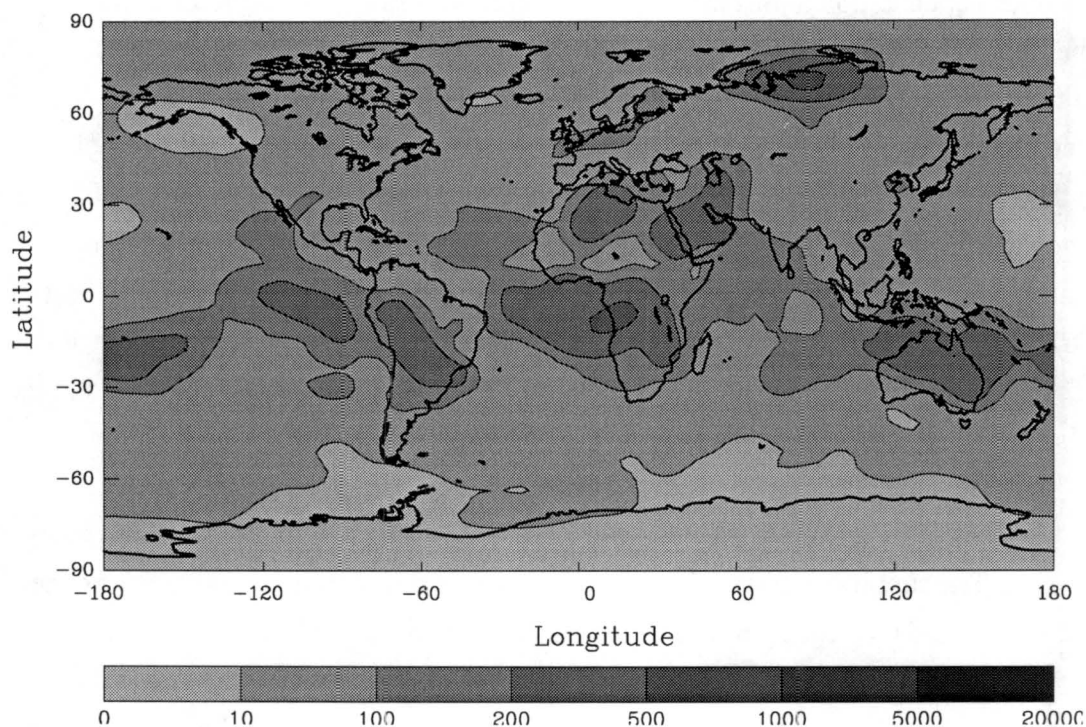


Figure 12. Total aerosol number concentration [cm^{-3}] at the surface for sensitivity study using the alternate aqueous chemistry timestep.

In the present formulation, the addition of the aqueous sulfate mass to mode 2 normally modifies only the mass of the mode 2 particles. There is a special case, however, for which this aqueous sulfate mass addition can modify the number in mode 2. If this mass is added to a parcel which has no particles in mode 2, a diameter is assumed, and a corresponding number concentration is computed by dividing the aqueous mass into particles of that diameter. Applying this source rate over three hours can lead to a large number of particles, if the parcel in question is free of particles to begin with. Applying the aqueous mass addition every hour leads to a smoother addition of this large sulfuric acid mass source, since after the first addition of mode 2 number, subsequent mass additions can be added to those particles instead of creating new ones. This is the primary reason for the differences between the predictions shown in Fig. 12 and those in Fig. 5c.

6. *Future work*

The obvious next addition to this model is a background aerosol distribution for the continents and the oceans, and a representative aerosol source rate over the continents. These two parameters will be used to account for particle number concentration not produced by homogeneous nucleation, and to keep track of the amount of sulfuric acid vapor taken up by the background aerosol, which reduces the amount of vapor available for homogeneous nucleation. It is expected that the revised predicted global aerosol number concentration map (Fig. 5c) will approximate observations more closely, especially near industrialized regions, if appropriate source strengths of the background aerosol species are applied. In particular, organic aerosols and aerosol precursor gases should be added to the model, since these are frequently a major component of the fine aerosol mass.

Additional sensitivity testing of the code will be done by using a diurnally varying vapor source rate. The simplest approach is to approximate the diurnal variation by varying the diurnally-averaged OH· concentration depending on whether it is night or day. That is, at any given grid point, the average OH· value follows a sinusoidal variation, with peak values equal to twice those used here. This will integrate to the same total monthly oxidation of sulfur gases, but will somewhat change the spatial distribution of the precursors and their products. The biggest impact, however, will be on the aerosol model predictions, since the increased vapor production rate will enhance the gas-to-particle conversion processes of nucleation and condensation. It is known that the number concentration of aerosol predicted from a diurnally-varying vapor source rate will not be the same as that predicted from a diurnally-averaged source rate, and will in fact average to higher number concentrations, with larger amplitude in the maxima and minima of N . The sensitivity of N to the assumed nucleation rate formulation should also be tested by introducing some alternative nucleation rate formulas.

The treatment of the aqueous-path pathway in both the chemical and in the microphysical aspects of the model is an area for improvement. The chemical source rates should ideally be linked to the presence and type of cloud, and the concentrations of major oxidants such as hydrogen peroxide and ozone. The interactions between this chemical source and the increase in mass of particles which serve as CCN also need further development and sensitivity testing. The importance of this source in the total budgets of the sulfur species places a high priority on development efforts in this area.

7. *Summary and conclusions*

A simple model of aerosol formation and evolution has been implemented and tested in a global transport, transformation and deposition model. The application presented here uses only sulfur chemistry to drive the formation of aerosol precursors and does not include any primary particulate emissions or sources of particulate mass other than sulfur. The aerosol precursor, sulfuric acid, is partitioned between the gas and particulate phases by the aerosol microphysics model. The computational feasibility of the coupled chemistry / aerosol model has been established by streamlining and optimizing the aerosol model calculations. Although results from the model are reasonable in the light of its current status, with improved aerosol information, specifically a background aerosol distribution and aerosol sources, predictions from the global model should more closely match observations.

The preliminary results shown here indicate that surface particle number concentrations, particularly in continental regions, are most strongly controlled by primary emissions from the surface. In contrast, the clean maritime aerosol is less strongly controlled by such sources, although some regions, such as the North Atlantic, are heavily impacted and are not well represented by the current model. At upper tropospheric levels (355 mb), the predicted aerosol number concentrations are in reasonable agreement with observations, suggesting that surface sources of number are less important in regulating the aerosol microphysics at higher levels of the atmosphere.

A case study was presented which followed the transport of a parcel from the Atlantic marine boundary layer to 300 mb, and its subsequent return to the surface in subsidence over northern Africa. Several thousand particles cm^{-3} were nucleated in this parcel as it was lifted to the upper troposphere after contact with sulfur emissions advecting off the North American continent. These particles largely survived until they were transported to the surface in subsiding air. While this case study is a rather specialized example, it does support the concept of the free troposphere as a source of particle number to the boundary layer.

The results of the model are highly dependent upon the choice of chemical system, the choice of nucleation rate expression for the formation of new particles from the gas phase, and the treatment of other gas-to-particle conversion processes such as condensation of vapor and addition of sulfate mass created via heterogeneous pathways. The results presented here are not intended to represent a fully realized formulation of the complex

atmospheric aerosol system, or even the sulfate aerosol fraction thereof. They are, however, a first step in adding prognostic aerosol equations to a large-scale model. The model calculations also provide insight into the nature of the relationships between aerosol mass and number concentration in the atmosphere, and suggest which processes are most important and should receive highest priority in further model development.

Acknowledgments

This material is based upon work supported by the National Science Foundation under Grant No. ATM-9215951. Special thanks is extended to Hal Eddleman for his assistance.

References

- Andreae, M. O., R. J. Ferek, F. Bermond, K. P. Byrd, R. T. Engstrom, S. Hardin, P. D. Houmère, F. LeMarrec, H. Raemdonck and R. B. Chatfield (1985). Dimethyl sulfide in the marine atmosphere: A global view. *Science* **90**: 744-747.
- Arimoto, R., R. A. Duce, D. L. Savoie and J. M. Prospero (1992). Trace elements in aerosol particles from Bermuda and Barbados: Concentrations, sources and relationships to aerosol sulfate. *Journal of Atmospheric Chemistry* **14**: 439-457.
- Ayers, G. P., R. W. Gillett and J. L. Gras (1980). On the vapor pressure of sulfuric acid. *Geophysical Research Letters* **7**: 433-436.
- Ayers, G. P., J. P. Ivey and R. W. Gillett (1991). Coherence between seasonal cycles of dimethylsulphide, methanesulfonate and sulphate in marine air. *Nature* **349**: 404-406.
- Binkowski, F. S., and U. Shankar (1995). The regional particulate matter model: Part I, Model description and preliminary results. *Journal of Geophysical Research* (in press).
- Charlson, R. J., J. Langner, H. Rodhe, C. B. Leovy and S. G. Warren (1991). Perturbation of the northern hemisphere radiative balance by backscattering from anthropogenic sulfate aerosols. *Tellus* **43AB**(4): 152-163.
- Chuang, C. C. and J. E. Penner (1994). Effects of anthropogenic sulfate on cloud drop nucleation and optical properties. Lawrence Livermore National Laboratory Internal Report UCRL-JC-114084, Livermore CA.
- Clarke, A. D. (1992). Atmospheric nuclei in the remote free-troposphere. *Journal of Atmospheric Chemistry* **14**: 479-488.
- d'Almeida, G. A., P. Koepke and E. P. Shettle (1991). Atmospheric aerosols: Global climatology and radiative characteristics. A. Deepak Publishing, Hampton, Virginia.

- Eisele, F. L. and D. J. Tanner (1993). Measurement of the gas phase concentration of H_2SO_4 and methane sulfonic acid and estimates of H_2SO_4 production and loss in the atmosphere. *Journal of Geophysical Research* **98**(D5): 9001-9010.
- Erickson, D. J., J. J. Walton, S. J. Ghan and J. E. Penner (1991). Three-dimensional modeling of the global atmospheric sulfur cycle: A first step. *Atmospheric Environment* **25A**(11): 2513-2520.
- Fitzgerald, J. W. (1991). Marine aerosols: a review. *Atmospheric Environment* **25A**(3/4): 533-545.
- Galloway, J. N., J. E. Penner, C. S. Atherton, D. R. Hastie, J. M. Prospero, H. Rodhe, R. S. Artz, Y. J. Balkanski, H. G. Bingemer, and R. A. Brost (1992). Sulfur, nitrogen, and oxidant levels in the North Atlantic Ocean's atmosphere: A synthesis of field and modeling results. *Global Biogeochemical Cycles* **6**: 77-100.
- Hegg, D. A. and P. V. Hobbs. (1980). Measurements of gas-to-particle conversion in the plumes from five coal-fired electric power plants. *Atmospheric Environment* **14**: 99-116.
- Heintzenberg, J., J. A. Ogren, S.-A. Odh, L. Backlin and T. Danielsen (1991). The MISU baseline station. Department of Meteorology, Stockholm University. Report AA-02.
- Hoppel, W. A., J. W. Fitzgerald, G. M. Frick, R. E. Larson and E. J. Mack (1990). Aerosol size distributions and optical properties found in the marine boundary layer over the Atlantic Ocean. *Journal of Geophysical Research* **95**(D4): 3659-3686.
- Jaeger-Voirol, A. and P. Mirabel (1989). Heteromolecular nucleation in the sulfuric acid-water system. *Atmospheric Environment* **23**(9): 2053-2057.
- Jensen, T. L., S. M. Kreidenweis, Y. Kim, H. Sievering, and A. Pszenny (1996). Aerosol distributions measured in the North Atlantic marine boundary layer during ASTEX/MAGE. *Journal of Geophysical Research* (in press).
- Kerminen, V.-M., Anthony S. Wexler (1994). Post-fog nucleation of H_2SO_4 - H_2O particles in smog. *Atmospheric Environment* **28**(15): 2399-2406.
- Kiehl, J. T. and B. P. Briegleb (1993). The relative roles of sulfate aerosols and greenhouse gases in climate forcing. *Science* **260**: 311-314.
- Kreidenweis, S. M., F. D. Yin, S. C. Wang, D. Grosjean, R. C. Flagan and J. H. Seinfeld (1991). Aerosol formation during photooxidation of organosulfur species. *Atmospheric Environment* **25A**(11): 2491-2500.
- Langner, J. and H. Rodhe (1991). A global three-dimensional model of the tropospheric sulfur cycle. *Journal of Atmospheric Chemistry* **13**: 225-263.
- Levy, H., J. N. Galloway, A. Eliassen, B. E. A. Fischer, K. Gorzelska, D. R. Hastie, J. L. Moody, A. G. Ryaboshapko, D. Savoie and D. M. Whelpdale (1990). The long-range transport of sulfur and nitrogen compounds. The Long-Range Atmospheric

- Transport of Natural and Contaminant Substances. Editor A. H. Knap. Kluwer Academic Publishers, Dordrecht. pp 231-257.
- Malm, W. C., J. F. Sisler, D. Huffman, R. A. Eldred and T. A. Cahill (1994). Spatial and seasonal trends in particle concentration and optical extinction in the United States. *Journal of Geophysical Research* **99**(D1): 1347-1370.
- Nguyen, G. P., N. Mihalopoulos, and S. Belviso (1990). Seasonal variation of atmospheric dimethylsulfide at Amsterdam Island in the Southern Indian Ocean. *Journal of Atmospheric Chemistry* **11**: 123-142.
- Novakov, T. and J. E. Penner (1993). Large contribution of organic aerosols to cloud condensation nuclei concentrations. *Nature* **365**: 823-826.
- Pastukhov, B. V. (1991). Background concentrations of sulphur dioxide and sulphate in boundary layer of the atmosphere. Monitoring of Background Pollution of Environment. Editor F. Y. Rovinwky. Gidrometeoizdat Publishing House, Leningrad. pp 10-22.
- Penner, J. E., C. S. Atherton and T. E. Graedel (1994a). Global emissions and models of photochemically active compounds. Global Atmospheric-Biospheric Chemistry. Editor R. G. Prinn. Plenum Press, New York. pp 223-247.
- Penner, J. E., R. J. Charlson, J. M. Hales and N.S. Laulainen, R. Lefier, T. Novakov, J. Ogren, L. F. Radke, S. E. Schwartz, and L. Travis (1994b). Quantifying and minimizing uncertainty of climate forcing by anthropogenic aerosols. *Bulletin of the American Meteorological Society* **75**(3): 375.
- Raes, F., A. Saltelli and R. Van Dingenen (1992). Modelling formation and growth of H₂SO₄-H₂O aerosols: Uncertainty analysis and experimental evaluation. *Journal of Aerosol Science* **23**(7): 759-771.
- Savoie, D. L. and J. M. Prospero (1989). Comparison of oceanic and continental sources of non-sea-salt sulphate over the Pacific Ocean. *Nature* **339**: 685-689.
- Savoie, D. L., J. M. Prospero, R. J. Larsen and E. S. Saltzman (1992). Nitrogen and sulfur species in aerosols at Mawson, Antarctica, and their relationship to radionuclides. *Journal of Atmospheric Chemistry* **14**: 181-204.
- Savoie, D. L., J. M. Prospero and E. S. Saltzman (1989). Non-sea-salt sulfate and nitrate in trade wind aerosols at Barbados: evidence for long-range transport. *Journal of Geophysical Research* **94**(D4): 5069-5080.
- Schaug, J., J. E. Hanssen, K. Nodop, B. Ottar and J. M. Pacyna (1987). Summary report from the chemical co-ordinating centre for the third phase of EMEP. The Norwegian Institute for Air Research. EMEP/CCC-report 3/87.
- Seinfeld, J. H. (1986). Atmospheric chemistry and physics of air pollution. New York, John Wiley & Sons.
- Shaw, R. W. J. and R. J. Paur (1983). Measurements of sulfur gases and particles during sixteen months in the Ohio River Valley. *Atmospheric Environment* **17**: 1431-1438.

- Walton, J. J., M. C. MacCracken and S. J. Ghan (1988). A global-scale Lagrangian trace species model of transport, transformation, and removal processes. *Journal of Geophysical Research* **93**(D7): 8339-8354.
- Warren, D. R. and J. H. Seinfeld (1984). Nucleation and growth of aerosol from a continuously reinforced vapor. *Aerosol Science and Technology* **3**: 135-153.
- Weber, R. J., P. H. McMurry, F. L. Eisele, D. J. Tanner (1995). *Journal of Atmospheric Science* (in press).
- Wuebbles, D. J., P. S. Connell, K. E. Grant, R. Tarp, K. E. Taylor (1987). Initial results with the LLNL 2-D chemical-radiative-transport model of the troposphere and stratosphere. Lawrence Livermore National Laboratory Internal Report UCID-21178, Livermore CA.
- Wyslouzil, B. E., J. H. Seinfeld, R. C. Flagan and K. Okuyama (1991). Binary nucleation in acid-water systems. II. Sulfuric acid-water and a comparison with methanesulfonic acid-water. *Journal of Chemical Physics* **94**(10): 6842-6850.
- Youngblood, D. A., S. M. Kreidenweis (1994). Further Development and Testing of a Bimodal Aerosol Dynamics Model. Colorado State University, Department of Atmospheric Science, Report No. 550.

Appendix

A.1 Framework of calculations

The flowchart of operations has been shown in Figure 2 and is again briefly summarized here. After initialization of the model parameters, the chemical source rate of condensable vapor, H_2SO_4 , is determined each hour; the partitioning of this source rate between the vapor and the aerosol is accomplished within the aerosol subroutines. The first aerosol computation is a call to the merging subroutine. This routine simulates the transfer of mass and number from mode 1 to mode 2 and is called every hour. The next step is the condensation-nucleation calculations (vapor source partitioning, in addition to particle formation and growth) in which timesteps smaller than 1 hour are used. The third step is coagulation of aerosol particles and it is also done every hour. The final step is the addition of the aqueous mass to mode 2.

A.2 Condensational growth

The equation for particle growth by condensation (assuming spherical particles and negligible H_2SO_4 vapor pressure over the particle surface) is:

$$R_c = \frac{2\pi D_j p^\circ}{RT} \int_0^\infty D_p \beta(D_p) n(D_p) S, \quad (\text{A.1})$$

where D_j is the molecular diffusion coefficient, p° is the saturation vapor acidity, R is the universal gas constant, T is temperature, D_p is particle diameter, S is the vapor supersaturation, and β is a correction factor which extends the condensation rate expression through the transition and kinetic regimes. If it is assumed that particle size does not change significantly over a timestep, equation (A.1) reduces to:

$$R_c = \alpha 2\pi D_j V \overline{D_p} \beta(\overline{D_p}) N. \quad (\text{A.2})$$

where V is the H_2SO_4 vapor concentration, \overline{D}_p is the mean diameter, N is total particle number concentration, and α is a factor (<1) which accounts for the fact that the true aerosol distribution is polydisperse. Using this assumption and applying mass balance, the amount of H_2SO_4 remaining in the gas phase is calculated according to:

$$V(t) = \frac{R_g}{F_{tot}} + \left(V - \frac{R_g}{F_{tot}}\right) \exp(-F_{tot} \Delta t), \quad (\text{A.3})$$

where F_{tot} is the sum of the individual condensation coefficients:

$$F_{tot} = F_1 + F_2 = 2\pi D_j (\overline{D}_{p1} \beta(D_{p1}) N_1 + \overline{D}_{p2} \beta(D_{p2}) N_2), \quad (\text{A.4})$$

and R_g is the H_2SO_4 vapor source rate.

The vapor condensed onto particles is given by:

$$\Delta M = R_g \Delta t + V - V(t), \quad (\text{A.5})$$

which is divided between the two modes according to:

$$M_1(t + \Delta t) = M_1(t) + \left(\frac{F_1}{F_{tot}}\right) \Delta M, \text{ and} \quad (\text{A.6})$$

$$M_2(t + \Delta t) = M_2(t) + \left(\frac{F_2}{F_{tot}}\right) \Delta M. \quad (\text{A.7})$$

This concept is similar to that used by Kerminen and Wexler (1994).

A.3 Merging

Merging the two modes accounts for the growth of mode 1 particles into mode 2, conserving mass and particle number. This mechanism is necessary because the two modes act independently of each other, and may in fact grow to similar sizes, at which point they should be combined into a single mode. In this work, we assume the combined

mode is the accumulation mode. Two methods for merging the two modes were tested in the global model. The first method is based on an analysis of the condensation rates onto the separate modes and the merged mode:

$$\chi = \frac{R_{c1} + R_{c2}}{R_{cmerged}} = \frac{N_1 D_{p1} \beta_1 + N_2 D_{p2} \beta_2}{N_m D_{pm} \beta_m}. \quad (\text{A.8})$$

This calculation is compared with a preset criterion, which allows a certain amount of error to occur in the condensation rates as a result of the merge, and if that criterion is passed, mode 1 mass and number are transferred to mode 2. The nucleation mode is thus zeroed until the next occurrence of new particle formation.

The alternate merging mechanism is based on the following differential equation:

$$\frac{dN}{dt} = -\frac{N}{\tau_c}, \quad (\text{A.9})$$

where τ_c is the characteristic time for growth in mode 1:

$$\tau_c = \frac{H_2SO_4(g)}{R_{c1}}. \quad (\text{A.10})$$

The solution to (A.9) is:

$$N_{new} = N_{old} \exp\left(-\frac{\Delta t}{\tau_c}\right). \quad (\text{A.11})$$

where Δt is the timestep on which the condensational growth calculations are done.

Therefore, ΔN is:

$$\Delta N = N_{new} - N_{old} = N_{old} \left(\exp\left(-\frac{\Delta t}{\tau_c}\right) - 1 \right). \quad (\text{A.12})$$

This number of particles is transferred from mode 1 to mode 2, along with the associated mass, which is the mean mass per particle in mode 1 prior to transfer. This method accomplishes a continuous transfer of particle mass and number from the nucleation mode to the accumulation mode, accounting for particle growth. Therefore, this calculation is done wherever the condensational growth calculations are done.

A.4 Predicting the onset of nucleation

The nucleation rate of new sulfuric acid particles from the gas phase is a sensitive function of acid vapor concentrations, relative humidity, and temperature (Jaeger-Voirol and Mirabel, 1989). Therefore, predicting the onset of nucleation requires frequent updates and examination of the H_2SO_4 vapor concentration. In order to accomplish this, the chemistry-aerosol coupling timestep is subdivided into 300 second steps. At the beginning of the routine the nucleation sentinel, j_{nuc} , is set to zero, meaning that the possibility of nucleation has yet to be determined. The conditions existing in each parcel are then examined to see if the conditions for a nucleation burst, described in the next section, have been met.

For those parcels in which a nucleation burst has not yet been predicted, but has not been ruled out, the concentration for each of the three individual H_2SO_4 branches are advanced subject to equation (A.3).

Finally, given the change in total H_2SO_4 vapor, the total vapor source and the condensation rate coefficients for each mode, the change in mass for the two modes is computed, according to equations (A.6) and (A.7)

A.5 Nucleation

It is fairly well known (Kreidenweis *et al.*, 1991; Warren and Seinfeld, 1984) that homogeneous nucleation is only likely to occur in areas where the preexisting particle surface area is low and/or the vapor concentration and relative humidity are high. In the two-moment model, nucleation occurs when the vapor field exceeds a critical value. The critical value, V_{crit} , is a function of relative humidity, temperature, and the available vapor source rate:

$$V_{crit} = \hat{R}_g \exp(-0.7426x - 11.204), \quad (\text{A.13})$$

where \hat{R}_g is the source rate available for nucleation, which is the total chemical source rate reduced by the rate at which vapor is being condensed on pre-existing particles,

$$\hat{R}_g = R_g - R_{c1} - R_{c2} \quad (\text{A.14})$$

and x is a quantity correlated to relative humidity (RH), saturation acidity (pa0), and \hat{R}_g ,

$$x = \ln\left(\frac{\hat{R}_g}{pa0}\right) + \frac{(10RH - 7)}{2}. \quad (\text{A.15})$$

The nucleation parameterization used here, which was developed by Youngblood and Kreidenweis (1994), contrasts from those used in other models (Binkowski and Shankar, 1995; Kerminen and Wexler, 1994) in that the vapor source rates, in addition to the critical vapor concentration, are used to predict nucleated particle number concentrations.

The computed value of V_{crit} is compared to the current value of the H_2SO_4 vapor concentration. If H_2SO_4 is greater than 90% of V_{crit} , then the nucleation flag is set to yes and the time of the onset of nucleation, $tnuc$, is set to the current time.

The computed value of the number and mass of nucleated particles has been parameterized in terms of J_{crit} and Δt_b where J_{crit} is calculated from the current values of V_{crit} , RH , and temperature, and Δt_b is a function of V_{crit} , J_{crit} , RH and temperature (Youngblood and Kreidenweis, 1994). The amount of this Δt_b for which the burst is allowed to continue is limited by the portion of the coupling timestep (1 hour) remaining in the cycle, Δt_{cycle} . For example, if a burst starts at 3500 seconds and has a 1000 second duration, it will only be allowed to continue for 100 seconds. The resulting mass and number added to mode 1 as a result of the nucleation burst are:

$$M_1 = \hat{R}_g \Delta t_b, \quad (\text{A.16})$$

and

$$N_1 = J_{crit} \Delta t_{nuc}, \quad (\text{A.17})$$

where,

$$\Delta t_{nuc} = \min(\Delta t_b, \Delta t_{cycle}). \quad (\text{A.18})$$

In addition, there is an increase of mass in both modes that occurs because of condensation that goes on concurrently with the nucleation burst.

In the case of a burst that is not completed before the end of an aerosol cycle timestep, is possible that the state of the parcel will be such that the prematurely-ended burst will continue at the beginning of the next aerosol cycle, but there is no guarantee of this.

A.6 Coagulation

Coagulation calculations are done to account for collisions between particles within mode 1, within mode 2, and between the two modes. Intramodal coagulation reduces number in a given mode and conserves mass, while intermodal coagulation reduces particle number and mass in mode 1 and increases particle mass in mode 2.

In this parameterization, Brownian coagulation within each mode is computed only if the number of particles in the given mode exceeds some critical number. The critical number is based on the characteristic times derived from the analytical solution of the differential coagulation equation, assuming monodisperse particles and a constant coagulation coefficient:

$$\frac{dN}{dt} = -\frac{1}{2}KN^2. \quad (\text{A.19})$$

The characteristic time for this process is:

$$\tau_c = \frac{2}{KN}. \quad (\text{A.20})$$

If this characteristic time is 10 times larger than the coupling timestep, then coagulation within a given mode is not considered. For simplicity, the coefficient, K , for coagulation within a given mode is assumed to be a constant value of $1.e-9 \text{ cm}^3 \text{ s}^{-1}$ (Seinfeld, 1986). Based on a 3600 second coupling timestep and equation (A.20), if N is less than $5.6 \times 10^4 \text{ cm}^{-3}$, then coagulation within that given mode will have a negligible effect on N over the timestep and is not computed.

For coagulation between the two modes, the differential equation is:

$$\frac{dN_1}{dt} = -KN_1N_2, \quad (\text{A.21})$$

with a corresponding characteristic time of,

$$\tau_c = \frac{1}{K_{12}N_{2crit}}. \quad (\text{A.22})$$

Therefore, if

$$K_{12}N_{2crit} \leq \tau_c^{-1}, \quad (\text{A.23})$$

then the characteristic time is too long for coagulation to appreciably affect the number concentrations in either mode, and coagulation between the two modes is neglected. In this case, a constant value of K_{12} cannot be assumed because it varies over 6 orders of magnitude (Seinfeld, 1986). K_{12} was calculated for D_{p1} and D_{p2} between 0.001 and 100 μm . For a given diameter ratio, the maximum K_{12} value was chosen for use in the criterion; the maximum value was used to underestimate N_{2crit} such that cases for which coagulation might significantly effect N_1 and N_2 would not be neglected. Fits were then obtained for N_{2crit} as a function of diameter ratio, yielding, for a 3600 s coupling timestep: